Creation of a Genetic Calcium Channel Blocker by Targeted Gem Gene Transfer in the Heart

Mitsushige Murata, Eugenio Cingolani, Amy D. McDonald, J. Kevin Donahue, Eduardo Marbán

Abstract—Calcium channel blockers are among the most commonly used therapeutic drugs. Nevertheless, the utility of calcium channel blockers for heart disease is limited because of the potent vasodilatory effect that causes hypotension, and other side effects attributable to blockade of noncardiac channels. Therefore, focal calcium channel blockade by gene transfer is highly desirable. With a view to creating a focally applicable genetic calcium channel blocker, we overexpressed the ras-related small G-protein Gem in the heart by somatic gene transfer. Adenovirus-mediated delivery of Gem markedly decreased L-type calcium current density in ventricular myocytes, resulting in the abbreviation of action potential duration. Furthermore, transduction of Gem resulted in a significant shortening of the electrocardiographic QTc interval and reduction of left ventricular systolic function. Focal delivery of Gem to the atrioventricular (AV) node significantly slowed AV nodal conduction (prolongation of PR and AH intervals), which was effective in the reduction of heart rate during atrial fibrillation. Thus, these results indicate that gene transfer of Gem functions as a genetic calcium channel blocker, the local application of which can effectively modulate cardiac electrical and contractile function. **(*Circ Res.* 2004;95:398-405.)**

Key Words: calcium channel blocker ■ gene therapy

Intracellular Ca^{2+} plays a pivotal role in diverse biological processes, including gene regulation, memory, and cell death.[1,2] In the heart, Ca^{2+} is essential as the activator of muscle contraction.[3] Although Ca^{2+} is vital for normal function, excessive increases in intracellular Ca^{2+} foster arrhythmias, hypertrophy, apoptosis, and cardiac remodeling. Modulation of Ca^{2+} homeostasis could be useful for the therapeutic manipulation of such pathophysiological processes.[4-6] Among the cell's many Ca^{2+} handling proteins, the L-type calcium channel, initiating excitation-contraction coupling, represents a logical target for intervention. Indeed, in animal experiments, calcium channel blockers reduce cardiac hypertrophy in spontaneously hypertensive rats,[7] and inhibit the electrical remodeling induced by rapid atrial pacing.[8] Unfortunately, the use of calcium channel blockers is often accompanied by side effects (eg, hypotension, heart block, constipation),[6] which limits their utility for the treatment of heart disease. It would be highly desirable to be able to achieve calcium channel blockade in the heart (or part of the heart) without affecting other tissues.

Such a motivation prompted us to establish a novel method to modulate calcium channel activity focally. This was accomplished by viral gene transfer of Gem into the heart in vivo. Gem is a member of a small GTP-binding family of proteins within the Ras superfamily,[9,10] and was recently found to suppress L-type calcium currents in PC12 cells by inhibiting the trafficking of calcium channel α subunits to the plasma membrane.[11] Reasoning that a similar effect might be recruitable in native heart cells, we transduced an adenovirus encoding Gem into the heart, resulting in the suppression of L-type calcium currents and a concomitant reduction of cardiac contractility, as expected with cardiac-specific calcium channel blockade. As proof of principle for the value of focal Ca^{2+} channel blockade in vivo, we demonstrated that Gem was effective in slowing atrioventricular (AV) conduction when delivered into the porcine AV node, resulting in the reduction of heart rate during atrial fibrillation.

Materials and Methods

Plasmid Construction and Adenovirus Preparation

The full-length coding sequences of Gem (kindly supplied by Dr Katherine Kelly, NIH, Bethesda, Md, and independently by Dr Susumu Seino, Chiba, Japan) was cloned into the multiple cloning site of the adenovirus shuttle vector pAdCIG to generate pAdCIG-Gem. This construct is bicistronic (through an internal ribosome entry site) driven by a cytomegalovirus promoter and carrying green fluorescent protein (GFP) as a reporter. The point mutation W269G

Original received April 1, 2004; revision received June 24, 2004; accepted June 28, 2004.

From the Institute of Molecular Cardiobiology and Division of Cardiology, Department of Medicine, The Johns Hopkins University, Baltimore, Md.

Under a licensing agreement between Exeigen, Inc. and the Johns Hopkins University, Drs Marbán, Donahue, and Murata are entitled to a share of royalty and milestone payments received by the University on sales of products described in this article. Drs Marbán and Donahue own Exeigen, Inc. stock, which is subject to certain restrictions under University policy. Drs Marbán and Donahue also are paid consultants to Exeigen, Inc. and paid members of the company's scientific advisory board. The terms of this arrangement are being managed by the Johns Hopkins University in accordance with its conflict of interest policies.

This manuscript was sent to Michael Rosen, Consulting Editor, for review by expert referees, editorial decision, and final disposition.

Correspondence to Eduardo Marbán, MD, PhD, Institute of Molecular Cardiobiology, The Johns Hopkins University, 720 Rutland Ave, Ross 844, Baltimore, MD 21205. E-mail marban@jhmi.edu

Circulation Research is available at http://www.circresaha.org DOI: 10.1161/01.RES.0000138449.85324.c5

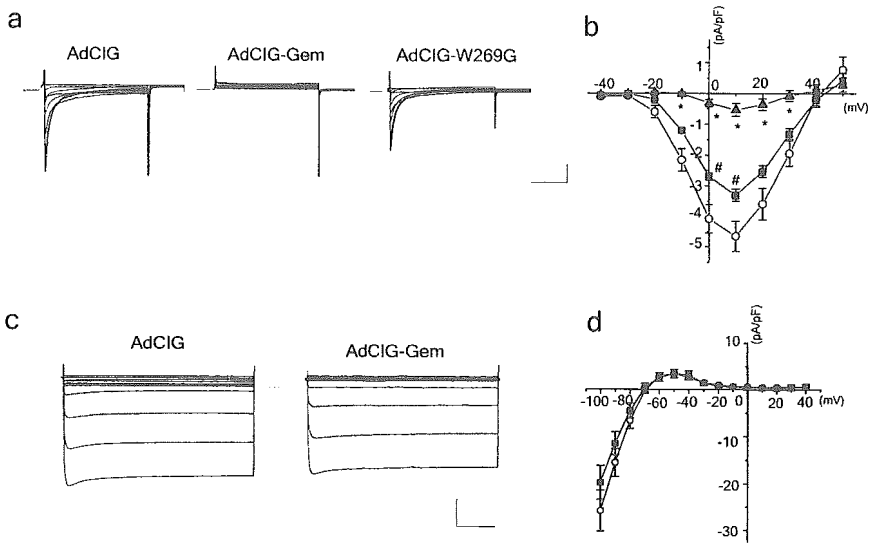

Figure 1. Effect of Gem on electrical properties in guinea-pig ventricular cardiomyocytes. a, Representative L-type calcium currents in an AdCIG-transduced (control), an AdCIG- wild type (WT) Gem-transduced, and an AdCIG-W269G mutant-transduced cell. Vertical scale bar=1 pA/pF; horizontal scale bar=100 ms; dash marks designate zero current. b, Current-voltage relationships of L-type calcium currents in control, AdCIG-WT Gem-transduced, and W269G mutant-transduced cells. L-type calcium current densities are significantly reduced in AdCIG-WT Gem-transduced cells (▲, n=8), compared with control cells (○, n=11), whereas W269G mutant had a slight effect (■, n=10). #$P<0.05$ vs control, *$P<0.01$ vs control. c, Representative I_{k1} currents in an AdCIG-transduced (control) and an AdCIG wild-type (WT) Gem-transduced cell. Vertical scale bar=10 pA/pF; horizontal scale bar=100 ms; dash marks designate zero current. d, Current-voltage relationships of I_{k1} currents in control (○, n=11) and AdCIG-WT Gem-transduced cells (■, n=10). There was no significant difference in I_{k1} current densities between control and AdCIG-WT Gem-transduced cells.

was introduced into Gem by site-directed mutagenesis, creating the vector pAdCIG-Gem W269G. Detailed methods of adenovirus vector construction have been described.[12-14] In vivo adenoviral transduction into guinea-pig hearts was performed as described.[15] Adenoviruses (160 μL, equivalent to $\approx 3\times10^9$ plaque-forming units, pfu) were injected in the left ventricular (LV) cavity of guinea pigs (280 to 340 g), whereas the aorta and pulmonary artery were clamped for 50 to 60 seconds.

Myocyte Isolation and Electrophysiology

Seventy-two hours after gene delivery, myocytes were isolated from the left ventricles of guinea pigs, using enzymatic digestions as previously described.[13] Membrane currents and action potentials were recorded using whole-cell patch clamp with an Axopatch 200B amplifier (Axon Instruments, Foster City, Calif). All myocyte recordings were performed at 37°C. Cells were superfused in solution containing (in mmol/L) 140 NaCl, 5 KCl, 1 $MgCl_2$, 10 HEPES, 2 $CaCl_2$, and 10 glucose (pH 7.4 adjusted with NaOH). For $I_{Ca,L}$ recordings, the external solution was replaced with solution containing (in mmol/L) 140 cholineCl, 5 CsCl, 1 $MgCl_2$, 10 HEPES, 2 $CaCl_2$, and 10 glucose (pH 7.4 adjusted with CsOH), after establishing the whole-cell clamp mode. The micropipette electrode solution for $I_{Ca,L}$ was composed of (in mmol/L) 120 CsCl, 10 TEACl, 1 $MgCl_2$, 10 HEPES, 10 EGTA, and 5 MgATP. Action potentials and I_{K1} were recorded with an internal solution composed of (in mmol/L) 130 K-glutamate, 9 KCl, 1 $MgCl_2$, 10 Na-HEPES, 2 EGTA, and 5 Mg-ATP (pH 7.2 adjusted with KOH). L-type calcium currents were elicited by 300 ms-depolarizing steps from −40 to 60 mV in 10 mV increments. For action potential recordings followed by the measurement of nitrendipine-sensitive Ca^{2+} currents, the external solution contained (in mmol/L) NaCl 140, KCl 5, $CaCl_2$ 2, $MgCl_2$ 1.0, glucose 10, and HEPES 10 (pH 7.4 with NaOH), and the pipette solution contained (in mmol/L) K-glutamate 130, KCl 9.0, $MgCl_2$ 1.0, EGTA 2.0, Mg-ATP 5.0, and Na-HEPES 10 (pH 7.3 with KOH). After recording the action potential, currents were elicited by the standard pulse protocol for calcium currents as shown before and after application of 10 μmol/L nitrendipine, and subtracted currents were considered as nitrendipine-sensitive calcium currents. For I_{K1} recordings, $CaCl_2$ was reduced to 100 μmol/L, $CdCl_2$ (200 μmol/L) was added to block $I_{Ca,L}$, and I_{Na} was steady-state inactivated by using a holding potential of −40 mV. To obtain I_{K1} as a Ba^{2+}-sensitive current, currents recorded before and after the addition of Ba^{2+} (500 μmol/L) were subtracted.

Borosilicate glass pipettes were pulled and fire-polished to final tip resistances of 1 to 3 MΩ when filled with internal recording solution. Uncompensated capacitance currents in response to small hyperpolarizing voltage steps were recorded for off-line integration to measure cell capacitance. Cells were allowed >5 minutes to equilibrate after whole-cell access was obtained. Action potentials were initiated by short depolarizing current pulses (2 ms, 100 to 300 pA, 10% to 15% over the threshold) at every 3 seconds. APD was measured as the time from the overshoot to the indicated percentage of repolarization. A xenon arc lamp was used to view green fluorescent protein (GFP) fluorescence at 488/530 nm (excitation/emission). Transduced cells were recognized by their obvious green fluorescence.

To measure gating currents, ionic currents were blocked by adding 2 mmol/L $CdCl_2$ and 0.1 mmol/L $LaCl_3$ to the bath solution. Leaks and capacitative transients were subtracted by a $P/-4$ protocol from a −100 mV holding potential. Charge movement was quantified by calculating the area under the curve for each trace, using the steady-state level of the current as a baseline.

Electrocardiograms

Body surface electrocardiograms (ECGs) were recorded within 2 hours after operation (baseline) and 72 hours after adenovirus injection, as previously described.[13] Guinea pigs were anesthetized with isoflurane, and needle electrodes were placed under skin. Needle electrode positions were marked postoperatively on the skin to ensure exactly the same electrode position for 72-hour recordings. Measured QT intervals were corrected (QTc) for heart rate as previously described.[16]

Cardiac Hemodynamic Studies

Seventy-two hours after LV injection, guinea-pigs were anesthetized with isoflurane. The right carotid artery was isolated and a micromanometer catheter (Millar Instruments, Houston, Texas) was inserted via the right carotid artery and passed retrogradely into the left ventricle. Position was confirmed by the characteristic decrease in diastolic pressure that occurred with passage of the catheter across the aortic valve into the LV cavity, after which LV pressure and the first derivative of LV pressure (dP/dt) were recorded.

Focal Gene Transfer Into AV Node

Adenoviral gene transfer into AV node was performed as described.[17] Briefly, immediately before catheterization, domestic swine (25 to 30 kg) received 25 mg sildenafil orally. The right carotid artery, right internal jugular vein, and right femoral vein were accessed by sterile surgical technique, and introducer sheaths were

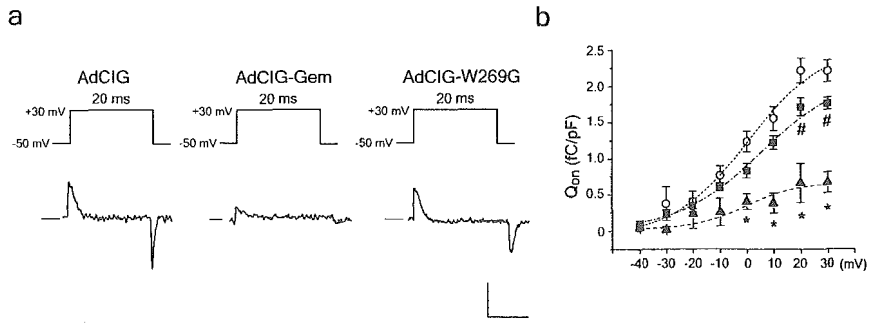

Figure 2. Effect of Gem on gating properties in guinea pig ventricular cardiomyocytes. a, Representative recordings of calcium channel gating current in an AdCIG-transduced (control), an AdCIG-WT Gem-transduced, and an AdCIG-W269G mutant-transduced cell. Vertical scale bar=2 pA/pF; horizontal scale bar=10 ms; dash marks designate zero current. b, Pooled data for calcium channel gating charge in control, AdCIG-WT Gem-transduced, and AdCIG-W269G mutant-transduced cells. Q vs V data were fit to a Boltzmann distribution using the following equation: $Q=Q_{max}/[1+\exp(V-V_{1/2})/k]$, where $V_{1/2}$ is the half maximum potential, k is the slope factor. Calcium channel gating charge was significantly reduced in AdCIG-WT Gem-transduced cells compared with control cells, whereas restored in AdCIG-W269G mutant-transduced cells. #<0.05 vs control, *P<0.01 vs control.

inserted into each vessel. After baseline EP study, the right coronary artery was catheterized via the right femoral artery. The AV nodal branch was selected with a 0.014-inch guide wire, over which a 2.7F infusion catheter was inserted into the AV nodal artery. The following solutions were infused through the catheter: 10 mL normal saline (NS) containing 5 μg VEGF165 and 200 μg nitroglycerin >3 minutes, 1 mL NS containing 1.0×10^{10} pfu adenovirus and 20 μg nitroglycerin >30 seconds, and 2.0 mL NS >30 seconds.

Western Blot Analysis

Expression of Gem protein in the heart was determined by the immunoblot technique. For this purpose, crude homogenates of the left ventricle were prepared, normalized for protein content, and SDS-PAGE was performed on 4% to 12% gradient gels.

Monoclonal anti-Gem antibody (gift from Dr Katherine Kelly, NIH, Bethesda, Md) was used as a primary antibody. A peroxidase-conjugated goat anti-mouse IgG (Amersham Biosciences, Uppsala, Sweden) was used as a secondary antibody. Signals were visualized with enhanced chemiluminescence.

Statistical Analysis

All the data shown are mean±SEM. Statistical differences were determined using repeated measures ANOVA and Student paired t test, where appropriate, and $P<0.05$ was considered to indicate statistical significance.

Results

Overexpression of Gem in Guinea Pig Ventricular Cardiomyocytes

We first investigated whether Gem overexpression could inhibit L-type calcium current ($I_{Ca,L}$) in guinea-pig ventricular cardiomyocytes. Adenoviruses were injected into the left ventricular (LV) cavity of guinea-pig hearts, and 3 days later, LV cells were isolated. Overexpression of AdCIG-wild-type (WT) Gem resulted in a dramatic decrease of $I_{Ca,L}$ from a peak density of 4.7±0.5 pA/pF at 10 mV (n=11) in AdCIG-transduced (control) cells to 0.5±0.2 pA/pF at 10 mV (n=8) in AdCIG-WT Gem-transduced cells (Figure 1a and 1b). The inhibitory effect of Gem on $I_{Ca,L}$ attributable to the prevention of interaction between α and β subunits of L-type calcium channels by scavenging β subunits.[11] Based on this, we examined the effect of the less-effective AdCIG-W269G mutant.[11] Overexpression of the AdCIG-W269G mutant reduced $I_{Ca,L}$ modestly, but significantly (30% inhibition versus control, 3.3±0.2 pA/pF at 10 mV, n=10).

Because Gem is a GTP binding protein possibly involved in many signal transduction pathways, it is possible that Gem might have effects such on other ion currents. We therefore investigated the effects on other ion currents such as I_{K1}, I_{Na}, and $I_{Ca,T}$ before and after Gem gene transfer. No changes in I_{K1} were observed (at −50 mV, 3.5±0.2 pA/pF, n=5 versus 3.4±0.9 pA/pF, n=5, in AdCIG-WT Gem-transduced, and AdCIG-transduced cells, respectively; Figure 1c and 1d). Additionally, neither I_{Na} (at −40 mV, 25.8±2.5 pA/pF, n=5 versus 26.5±3.2 pA/pF, n=6, in AdCIG-WT Gem-transduced, and AdCIG-transduced cells, respectively), nor $I_{Ca,T}$ (at −20 mV, 0.43±0.13 pA/pF, n=4 versus 0.42±0.17 pA/pF, n=5, in AdCIG-WT Gem-transduced, and AdCIG-transduced cells, respectively) were affected; thus, transduction of Gem appears to specifically affect L-type Ca^{2+} channels.

If, as previously proposed, Gem binds to β-subunits of calcium channels and thereby inhibits the trafficking of α-subunits to the plasma membrane,[11] a decrease in the number of functional channels would be predicted. To assess channel number electrophysiologically, we measured the gating charge attributable to L-type calcium channels and isolated the calcium channel–specific component using 10 μmol/L nitrendipine, a pharmacological calcium channel blocker.[18,19] Overexpression of AdCIG-WT Gem resulted in a marked reduction of nitrendipine-sensitive gating currents compared with control (Figure 2a and 2b). The gating currents during depolarization were integrated to calculate charge movements during depolarization (Q_{on}). Control Q_{on} was significantly greater than that in AdCIG-WT Gem-transduced myocytes (2.2±0.2 fC/pF at +30 mV, n=6, versus 0.67±0.1 fC/pF at +30 mV, n=6; P=0.001). The voltage dependence of Q_{on} was comparable in AdCIG-transduced (control) and AdCIG-WT Gem-transduced cells, as demonstrated by simultaneously fit Boltzmann distributions to the mean data sets, with $V_{1/2}$=0.5 mV, k=13.3 mV in control, and $V_{1/2}$=−0.3 mV, k=9.8 mV in AdCIG-WT Gem-transduced cells. AdCIG-W269G mutant only modestly affected these parameters (1.8±0.1 fC/pF at +30 mV, $V_{1/2}$=5.5 mV, k=15.5 mV, n=6). These results indicate that the number of functional calcium channels in the cell membrane is indeed decreased in Gem-transduced cells, compared with AdCIG-transduced (control) cells. Those channels that do make it to the surface, however, appear to have normal gating properties.

Next, we investigated the effects of Gem overexpression on action potentials in ventricular cardiomyocytes. Overexpression of AdCIG-WT Gem resulted in the abbreviation of action potential duration (APD) without any change in resting membrane potential (−84.6±0.4 mV versus −84.9±0.4 mV) or

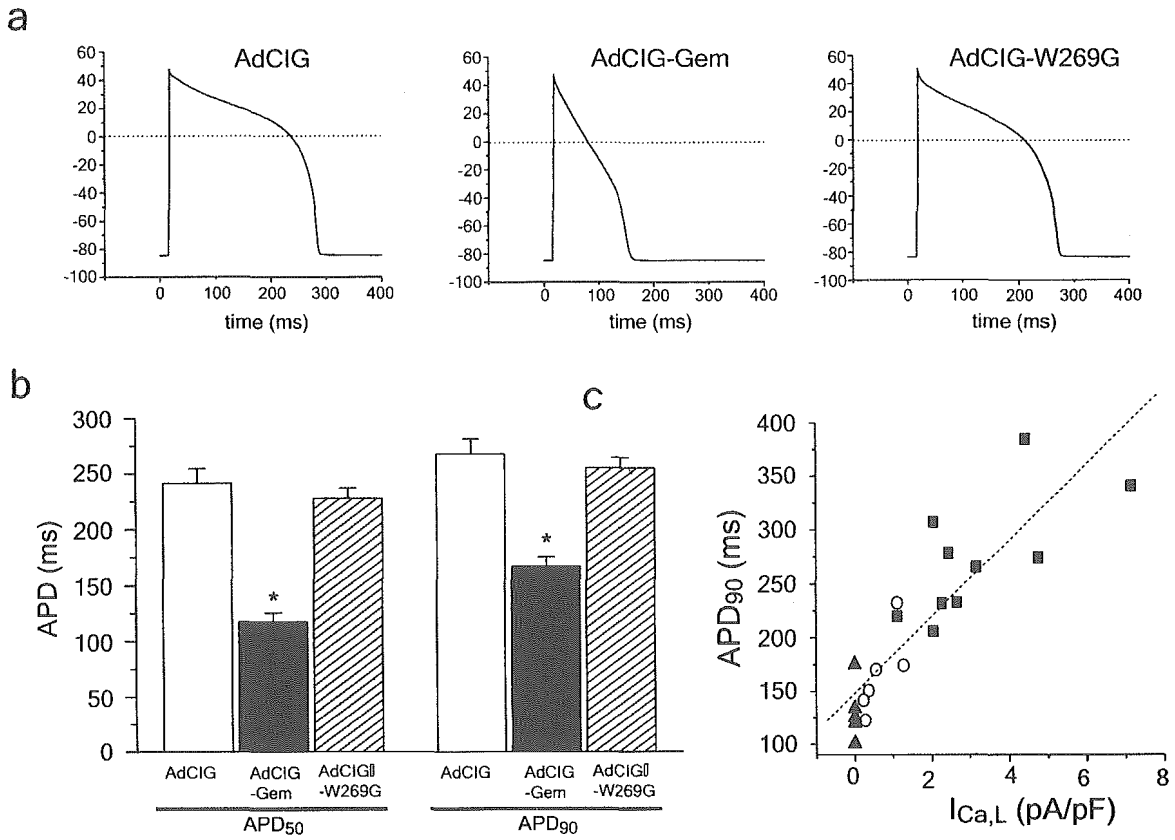

Figure 3. Effect of Gem on action potential in guinea pig cardiomyocytes. a, Representative action potentials in an AdCIG-transduced (control), an AdCIG-WT Gem-transduced cell, and an AdCIG-W269G mutant-transduced cell. Action potentials in AdCIG-WT Gem-transduced cells were abbreviated and lacked a robust plateau phase. b, Pooled data for action potential duration in control, AdCIG-WT Gem-transduced cells, and AdCIG-W269G mutant-transduced cells. Action potential duration was significantly reduced in AdCIG-WT Gem-transduced cells (n=12), compared with control cells (n=12), whereas restored in AdCIG-W269G mutant-transduced cells. *P<0.01 vs control (c). A highly significant correlation between APD_{90} and L-type calcium current density (r=0.866, P<0.0001). ■ indicates control (nitrendipine−); ○, AdCIG-WT Gem-transduced; ▲, control (nitrendipine+).

phase 0 depolarization (dV/dt_{max}) (−86.1±3.5 V/s versus −82.2±3.9 V/s) (Figure 3a). Both APD_{50} and APD_{90} were significantly shortened in AdCIG-WT Gem-transduced cells compared with control cells, whereas overexpression of AdCIG-W269G mutant had little effect (Figure 3a and 3b). Notably, the robust plateau phase was blunted in WT Gem-transduced myocytes.

The modification of action potentials became more pronounced as $I_{Ca,L}$ decreased. There was a clear correlation between $I_{Ca,L}$ density, calculated as the nitrendipine-sensitive ionic current, and APD_{90}; both were reduced in AdCIG-WT Gem-transduced myocytes compared with AdCIG-transduced (control) cells (n=21, r=0.87, P<0.0001) (Figure 3c).

In Vivo Phenotype of Cardiac Calcium Channel Blockade

We previously reported that the LV cavity injection method resulted in a transduction efficiency of 15% to 25% in the heart.[20] Western blot analysis (Figure 4a) confirmed Gem overexpression in all cardiac chambers, amounting to a 300±60% increase in the AdCIG-WT Gem-transduced animals relative to control levels (P=0.002). The presence of endogenous Gem in heart was unexpected, and gives reason to wonder whether it may play a physiological role in myocardial Ca^{2+} homeostasis; however, this possibility was not explored in the present study.

To assess the electrophysiological phenotype in intact animals, electrocardiograms were performed 3 to 4 days after injection of adenoviruses into the LV cavity. The QT interval[19] was shortened in AdCIG-WT Gem-transduced animals compared with AdCIG-transduced (control) animals (eg, Figure 4b). Consistent with action potential recordings in isolated AdCIG-WT Gem-transduced myocytes, the QTc intervals of the ECG measured 3 days after transduction were abbreviated in AdCIG-WT Gem-transduced animals compared with the same animals immediately after surgery (165±3.5 ms versus 148±2.3 ms, n=9; P<0.05). In contrast, no change in the QTc interval was observed in the animals transduced with AdCIG (165±3.3 ms versus 166±1.8 ms, n=6) or AdCIG-W269G mutant (166±1.8 ms versus 163±1.1 ms, n=7). Interestingly, we observed PQ interval prolongation in one of the AdCIG-WT Gem-transduced animals (central panel, Figure 4b), which was presumably induced by fortuitously intense expression of Gem in the AV node.

Effects of Gem on Cardiac Hemodynamics

Next, we examined the effect of WT Gem transduction on cardiac hemodynamics. Heart rate did not change (Figure 5a),

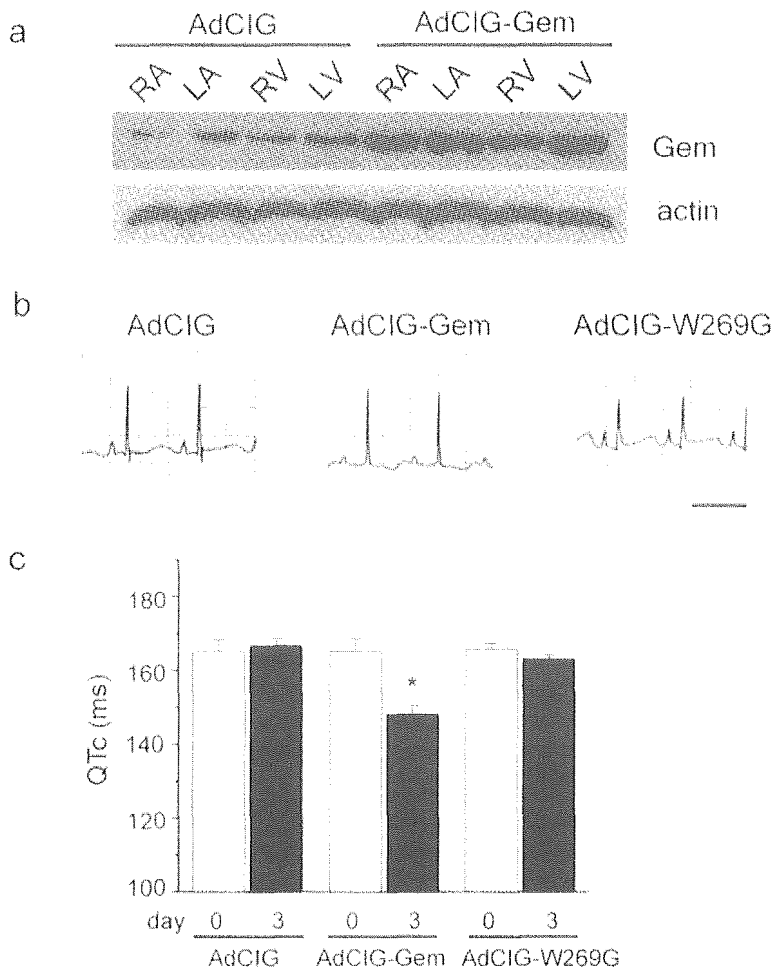

Figure 4. In vivo phenotype of cardiac calcium channel blockade by Gem transduction into guinea pig hearts. a, Western blot of heart tissue in each region (RA, LA, RV, LV) demonstrates Gem overexpression in the AdCIG-WT Gem transduced animals. b, EKG traces from an AdCIG-transduced (control), an AdCIG- WT Gem-transduced, and AdCIG-W269G mutant-transduced animal. QT interval was shortened, and the PQ interval was prolonged in an AdCIG-WT Gem transduced-animal, compared with a control animal as well as an AdCIG-W269G mutant-transduced animal. c, Pooled data for QTc interval calculated by a square root method. QTc interval was significantly shortened 3 days after gene delivery compared with that immediately after surgery in AdCIG-WT Gem-transduced animals, whereas there was no change in control as well as AdCIG-W269G mutant-transduced animals. *$P<0.01$ vs control.

but transduction of AdCIG-WT Gem resulted in the reduction of contractile activity in guinea pig hearts. The peak LV systolic pressure (LVSP) was reduced 3 days after gene delivery in AdCIG-WT Gem-transduced animals compared with AdCIG-transduced (control) animals (65.8±5.2 mm Hg, n=5, versus 85.8±2.7 mm Hg, n=4; $P<0.05$) (Figure 5b). Furthermore, the maximum first derivative of LV pressure (dP/dt_{max}) was reduced as well (4028±150 mm Hg/s, n=5, versus 4842±158 mm Hg/s, n=4; $P=0.01$) (Figure 5c). These data indicate that transduction of Gem produced a significant negative inotropic effect, as expected with myocardial calcium channel blockade.

Focal Modification of AV Nodal Conduction by Gem Gene Transfer

Atrial fibrillation is a disturbance of cardiac rhythm in which a rapid heart rate produces breathlessness and decreased exercise tolerance. Inhibition of AV nodal conduction, by calcium channel blockade, is the mainstay of drug therapy, but such therapy is fraught with side effects that are attributable to calcium channel blockade outside the AV node. We previously developed an intracoronary perfusion model for adenoviral gene delivery in pigs, and succeeded in the modification of AV nodal conduction by overexpression of the inhibitory G protein, Gαi2.[17] We reasoned that overexpression of Gem in the AV node would likewise slow AV nodal conduction, with possible benefit for rate control in atrial fibrillation. Seven days after gene transfer in the same swine model, AdCIG-WT Gem-transduced animals revealed prolongation of the PR interval on the surface ECG and the AH interval (but not the HV interval) on the intracardiac electrogram, confirming slowed conduction in the AV node (Figure 6b through 6e). During acute episodes of atrial fibrillation (Figure 6a), overexpression of AdCIG-WT Gem in the AV node caused a 20% reduction in the ventricular rate during atrial fibrillation (Figure 6f). This effect persisted in the setting of β-adrenergic stimulation as well as cholinergic inhibition (Figure 6g and the Table). Given the previous demonstration[17] that adenoviral transduction per se does not affect AV nodal conduction, we conclude that focal calcium channel blockade induced by Gem gene transfer into the AV node effectively reduces the heart rate in atrial fibrillation.

Discussion

The utility of calcium channel blockers for heart disease has been limited by potent vasodilatation and hypotension attributable to blockade of noncardiac channels. In this regard, gene therapy would be a feasible strategy for organ-specific or regionally specific treatment within an organ. In this study, we reported the novel finding that gene transfer of a ras-

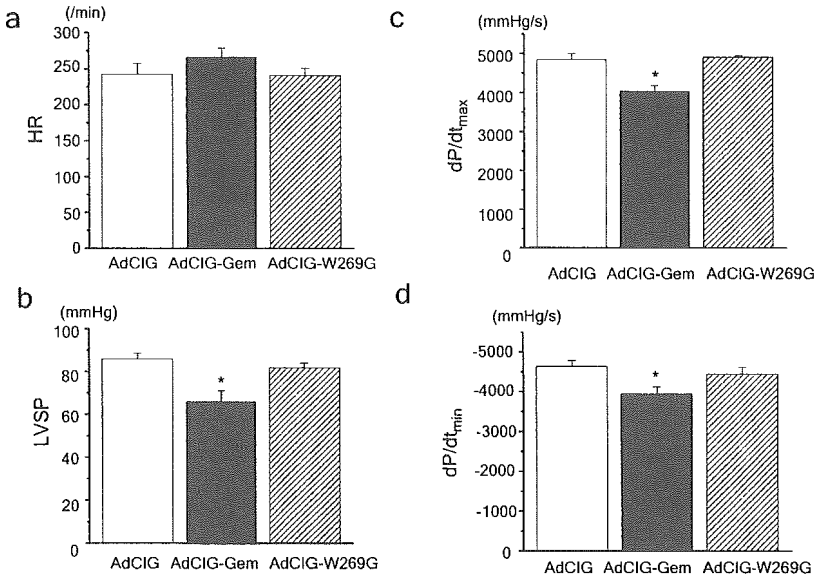

Figure 5. Effect of Gem on cardiac hemodynamics. Heart rate (HR) was not changed (a), and LV contractility (LVSP, dP/dt_{max}) (b and c) and relaxation (dP/dt_{min}) (d) were significantly reduced in AdCIG-WT Gem-transduced animals, compared with AdCIG- and AdCIG-W269G mutant-transduced animals.

related small G-protein, Gem could be useful as a genetic calcium channel blocker in the heart, expressed globally for the depression of contractility, or in part of the heart (the AV node), delivered focally to alter conduction.

Overexpression of AdCIG-WT Gem prominently inhibited $I_{Ca,L}$ in guinea-pig ventricular cardiomyocytes, resulting in marked abbreviation of APD, whereas W269G mutant had directionally similar but weaker effects. Furthermore, in vivo delivery of AdCIG-WT Gem shortened the QT interval, consistent with the abbreviation of APD seen in isolated cardiomyocytes. The prominent inhibitory effect of Gem WT on $I_{Ca,L}$ was effective in genetic modification of AV nodal conduction to treat atrial fibrillation, a common arrhythmia that afflicts >2 million Americans. Once AF becomes chronic, therapy is directed at achieving rate control with the use of AV nodal blocking agents.[21] Because $I_{Ca,L}$ underlies impulse conduction in the AV node, calcium channel blockers are preferred agents for rate control during AF, but often are not tolerated because of contractile depression from block of non-AV nodal calcium channels in the heart, or hypotension from block of noncardiac channels. In this study, we have achieved focal modification of AV nodal conduction by gene transfer of Gem WT via the AV nodal artery; the resultant regionally selective $I_{Ca,L}$ blockade is effective at rate control during AF, without undermining calcium channel function in the pumping chambers of the heart.

Based on the marked inhibitory effect of WT Gem on $I_{Ca,L}$, complete AV block might have been a potential consequence of WT Gem gene transduction. Anticipating this possibility, we introduced electronic pacemakers into all animals for backup purposes before gene transfer.

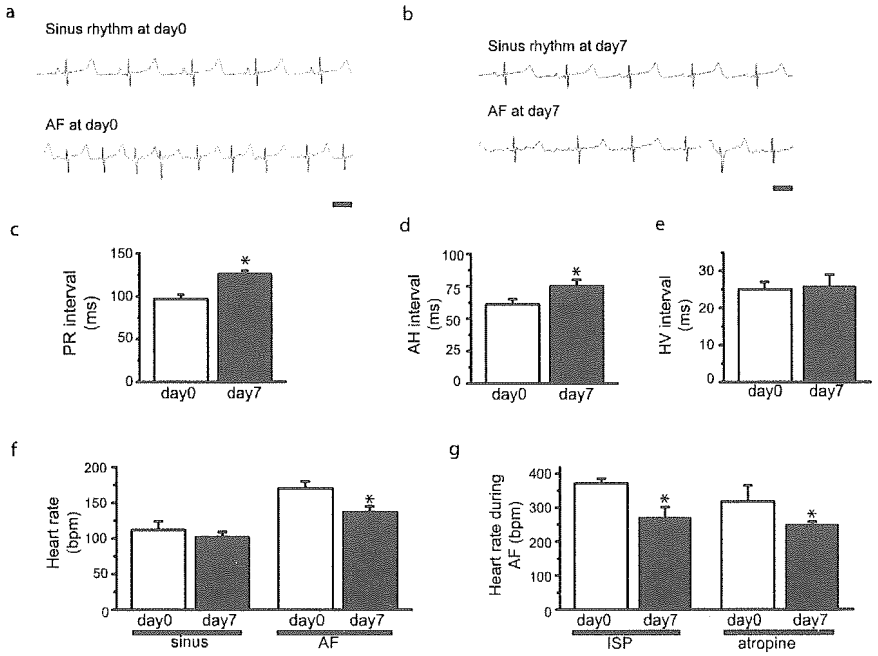

Figure 6. Focal modification of AV nodal conduction by WT Gem gene transfer in swine hearts. a, Representative ECG recordings during sinus rhythm and atrial fibrillation before gene transfer of WT Gem. Scale bar=200 ms. b, Representative ECG recordings during sinus rhythm and atrial fibrillation 7 days after gene transfer of WT Gem. Scale bar=200 ms. c, PR interval on the surface ECG before (day 0) and 7 days after transduction (day 7). *$P<0.05$ vs PR interval at day 0 (n=4). d, AH interval on the intracardiac electrogram before (day 0) and 7 days after transduction (day 7). *$P<0.05$ vs AH interval at day 0 (n=4). e, HV interval on the intracardiac electrogram before (day 0) and 7 days after transduction (day 7). f, Heart rate during sinus rhythm and atrial fibrillation before (day 0) and 7 days after transduction (day 7). *$P<0.05$ vs heart rate at day 0 (n=4). g, Heart rate during atrial fibrillation stimulated by isoproterenol (ISP) or atropine before (day 0) and 7 days after transduction (day 7). *$P<0.05$ vs heart rate at day 0 (n=4).

EP Parameters Before and 7 Days After Gene Transfer

	Day 0	Day 7	*P*
Heart rate during sinus rhythm, bpm	112±12	102±7	NS
ECG			
PR interval, ms	97±5	126±4	<0.01
QRS interval, ms	54±1	58±3	NS
QT interval, ms	314±15	320±17	NS
AH interval, ms	61±4	75±5	<0.05
HV interval, ms	25±2	26±3	NS
AVNERP, ms	238±23	265±19	NS
Heart rate during AF, bpm			
Baseline	170±10	137±8	<0.05
Isoproterenol	371±15	272±30	<0.05
Atropine	318±48	252±7	<0.05

Mean±SE, n=4 in each group

Nevertheless, AV conduction was significantly slowed without high-grade AV block. This effect is not inconsistent with the observed efficacy of gene transfer to the AV node (≈40% of AV nodal cells are transduced by our delivery method,[17] which might not suffice for complete AV block to develop.

A second application is for modulation of cardiac contractility. Hemodynamic studies showed that there was a significant negative inotropy in AdCIG-WT Gem-transduced hearts compared with AdCIG-transduced (control) hearts in guinea pigs, indicating that gene transfer of Gem could be useful to reduce cardiac contractility. Negative inotropic drugs are first-line treatment for patients with hypertrophic obstructive cardiomyopathy (HOCM),[22] to reduce contractile activity in the hypertrophic heart as a means of improving overall pumping efficacy. In accordance with this idea, iatrogenic myocardial infarction has been developed as another means of treating severe HOCM.[23–25] However, the utility of this radically destructive therapy is limited by its side effects, including inflammation, fibrosis, and arrhythmogenesis. Focal gene therapy may represent an attractive alternative approach to HOCM, in that part of the myocardium would be rendered regionally passive whereas remaining alive and excitable. More work will be necessary to reduce this idea to practice.

Although Gem is weakly expressed in the heart, its function has never been elucidated. In other cell types such as fibroblast and neurons, Gem was reported to interact with KIF9 and Rho kinase, resulting in changes in cell morphology and cytoskeletal organization.[26,27] We are now investigating Gem-mediated signal transduction pathways in cardiomyocytes, with a view to determining its potential utility in the suppression of hypertrophy. However, such data are beyond the scope of the present study.

The present study was designed for proof of concept. For such a purpose, adenoviruses are well-suited; they can be readily made and grown to high titers, they are highly effective at transducing cardiac myocytes, and they lead to intense expression of the transgene for days to weeks. Longer-term expression is limited with adenoviruses, and adverse effects have occurred clinically with their systemic use. Although our adenoviral transduction strategy should lead to higher expression in the heart, there could inevitably be some contaminated infection in other organs such as liver and kidney. For these reasons, other vectors such as adeno-associated virus or usage of a cardiac-specific promoter would be better-suited for chronic experiments, including those which will be required before the present approach can be translated to patients.

With the appropriate vector and delivery method, the present strategy is generalizable. If we can selectively block cardiac calcium channels, why not target arterioles to control hypertension as a durable surrogate for lifetime antihypertensive therapy? Might specific regions of the brain involved in memory benefit from local suppression of L-type channel activity? These and many other intriguing possibilities are now amenable to study by straightforward modifications of the novel approach described here.

Acknowledgments

This study was supported by the NIH (R37 HL36957 and P50 HL52307 to E.M.) and the Donald W. Reynolds Cardiovascular Clinical Research Center at Johns Hopkins. E.M. holds the Michel Mirowski, MD, Professorship of Cardiology. We thank B. O'Rourke, M.K. Leppo, and Peihong Dong for technical advice and helpful discussions.

References

1. Muth JN, Varadi G, Schwartz A. Use of transgenic mice to study voltage-dependent Ca^{2+} channels. *Trends Pharmacol Sci.* 2001;22:526–532.
2. Carafoli E, Santella L, Branca D, Brini M. Generation, control, and processing of cellular calcium signals. *Crit Rev Biochem Mol Biol.* 2001; 36:107–260.
3. Bers DM. Cardiac excitation-contraction coupling. *Nature.* 2002;415: 198–205.
4. Isner JM. Myocardial gene therapy. *Nature.* 2002;415:234–239.
5. Kaprielian R, del Monte F, Hajjar RJ. Targeting Ca^{2+} cycling proteins and the action potential in heart failure by gene transfer. *Basic Res Cardiol.* 2002;97:I136–45.
6. Missiaen L, Robberecht W, van den Bosch L, Callewaert G, Parys JB, Wuytack F, Raeymaekers L, Nilius B, Eggermont J, De Smedt H. Abnormal intracellular Ca^{2+} homeostasis and disease. *Cell Calcium.* 2000;28:1–21.
7. Feron O, Salomone S, Godfraind T. Action of the calcium channel blocker lacidipine on cardiac hypertrophy and endothelin-1 gene expression in stroke-prone hypertensive rats. *Br J Pharmacol.* 1996;118: 659–664.
8. Kurita Y, Mitamura H, Shiroshita-Takeshita A, Yamane A, Ieda M, Kinebuchi O, Sato T, Miyoshi S, Hara M, Takatsuki S, Ogawa S. Daily oral verapamil before but not after rapid atrial excitation prevents electrical remodeling. *Cardiovasc Res.* 2002;54:447–455.
9. Cohen L, Mohr R, Chen YY, Huang M, Kato R, Dorin D, Tamanoi F, Goga A, Afar D, Rosenberg N, et al. Transcriptional activation of a ras-like gene (kir) by oncogenic tyrosine kinases. *Proc Natl Acad Sci U S A.* 1994;91:12448–12452.
10. Maguire J, Santoro T, Jensen P, Siebenlist U, Yewdell J, Kelly K. Gem: an induced, immediate early protein belonging to the Ras family. *Science.* 1994;265:241–244.
11. Beguin P, Nagashima K, Gonoi T, Shibasaki T, Takahashi K, Kashima Y, Ozaki N, Geering K, Iwanaga T, Seino S. Regulation of Ca^{2+} channel expression at the cell surface by the small G-protein kir/Gem. *Nature.* 2001;411:701–706.
12. Hardy S, Kitamura M, Harris-Stansil T, Dai Y, Phipps ML. Construction of adenovirus vectors through Cre-lox recombination. *J Virol.* 1997;71:1842–1849.
13. Hoppe UC, Marban E, Johns DC. Distinct gene-specific mechanisms of arrhythmia revealed by cardiac gene transfer of two long QT disease genes. HERG and KCNE1. *Proc Natl Acad Sci U S A.* 2001;98:5335–5340.

14. Johns DC, Marx R, Mains RE, O'Rourke B, Marban E. Inducible genetic suppression of neuronal excitability. *J Neurosci.* 1999;19:1691–1697.
15. Mazhari R, Nuss HB, Armoundas AA, Winslow RL, Marban E. Ectopic expression of KCNE3 accelerates cardiac repolarization and abbreviates the QT interval. *J Clin Invest.* 2002;109:1083–1090.
16. Hayes E, Pugsley MK, Penz WP, Adaikan G, Walker MJ. Relationship between QaT and RR intervals in rats, guinea pigs, rabbits, and primates. *J Pharmacol Toxicol Methods.* 1994;32:201–207.
17. Donahue JK, Heldman AW, Fraser H, McDonald AD, Miller JM, Rade JJ, Eschenhagen T, Marban E. Focal modification of electrical conduction in the heart by viral gene transfer. *Nat Med.* 2000;6:1395–1398.
18. Bolger GT, Gengo PJ, Luchowski EM, Siegel H, Triggle DJ, Janis RA. High affinity binding of a calcium channel antagonist to smooth and cardiac muscle. *Biochem Biophys Res Commun.* 1982;104:1604–1609.
19. Bean BP. Nitrendipine block of cardiac calcium channels: high-affinity binding to the inactivated state. *Proc Natl Acad Sci U S A.* 1984;81:6388–6392.
20. Miake J, Marban E, Nuss HB. Functional role of inward rectifier current in heart probed by Kir2.1 overexpression and dominant-negative suppression. *J Clin Invest.* 2003;111:1529–1536.
21. Wyse DG, Waldo AL, DiMarco JP, Domanski MJ, Rosenberg Y, Schron EB, Kellen JC, Greene HL, Mickel MC, Dalquist JE, Corley SD. A comparison of rate control and rhythm control in patients with atrial fibrillation. *N Engl J Med.* 2002;347:1825–1833.
22. Spirito P, Seidman CE, McKenna WJ, Maron BJ. The management of hypertrophic cardiomyopathy. *N Engl J Med.* 1997;336:775–785.
23. Nielsen CD, Spencer WH, 3rd. Role of controlled septal infarct in hypertrophic obstructive cardiomyopathy. *Cardiol Rev.* 2002;10:108–118.
24. Sigwart U. Non-surgical myocardial reduction for hypertrophic obstructive cardiomyopathy. *Lancet.* 1995;346:211–214.
25. Chang SM, Nagueh SF, Spencer WH III, Lakkis NM. Complete heart block: determinants and clinical impact in patients with hypertrophic obstructive cardiomyopathy undergoing nonsurgical septal reduction therapy. *J Am Coll Cardiol.* 2003;42:296–300.
26. Piddini E, Schmid JA, de Martin R, Dotti CG. The Ras-like GTPase Gem is involved in cell shape remodelling and interacts with the novel kinesin-like protein KIF9. *EMBO J.* 2001;20:4076–4087.
27. Ward Y, Yap SF, Ravichandran V, Matsumura F, Ito M, Spinelli B, Kelly K. The GTP binding proteins Gem and Rad are negative regulators of the Rho- Rho kinase pathway. *J Cell Biol.* 2002;157:291–302.

Iron Chelation Suppresses Ferritin Upregulation and Attenuates Vascular Dysfunction in the Aorta of Angiotensin II–Infused Rats

Nobukazu Ishizaka, Kan Saito, Ichiro Mori, Gen Matsuzaki, Minoru Ohno, Ryozo Nagai

Objective—We have investigated whether long-term administration of angiotensin (Ang) II causes ferritin induction and iron accumulation in the rat aorta, and their possible relation to regulatory effects on gene expression and vascular function in Ang II-infused animals.

Methods and Results—Sprague-Dawley rats were given Ang II for 7 days via subcutaneously implanted osmotic minipumps. Ang II infusion caused a >20-fold increase in ferritin protein expression over control values. Immunohistochemistry showed that Ang II infusion markedly increased the ferritin expression in the aortic endothelial and adventitial cells, with some of the latter being identified as monocytes/macrophages. Prussian blue staining showed that stainable iron was observed in the adventitial layer of aorta from Ang II-infused animals, but not in the endothelial layer. Chelation of iron suppressed aortic induction of ferritin and also the oxidative stress markers, heme oxygenase-1 and 4-hydroxynonenal-modified protein adducts. In addition, iron chelation attenuated Ang II-induced impairment of aortic relaxations in response to acetylcholine and sodium nitroprusside and suppressed upregulation of mRNA levels of monocyte chemoattractant protein-1. Iron chelation also partially attenuated the medial thickening and perivascular fibrosis induced by Ang II infusion for 4 weeks.

Conclusion—Ang II infusion caused ferritin induction and iron deposition in the aortas. These phenomena might have a role in the regulation of gene expression, impairment of vascular function, and arterial remodeling induced by Ang II, which are presumably mediated in part by enhancement of oxidative stress. **(*Arterioscler Thromb Vasc Biol.* 2005;25:2282-2288.)**

Key Words: ferritin ■ heme oxygenase ■ hypertension ■ oxidative stress ■ vascular relaxation

Several previous studies have shown that ferritin expression is induced and iron accumulation is present in the atherosclerotic lesions in animal models and in humans.[1–5] The findings that treatment with iron chelators results in improved vascular endothelial function,[6,7] and that both iron chelation and restriction of iron intake reduce atheroma formation in atherosclerosis-prone animals[8,9] suggest that altered iron homeostasis in the body or in the vascular wall may play a role in the atherogenic processes and in impairment of vascular reactivity. The proposed mechanisms underlying iron-mediated vascular damage include platelet activation,[10] promotion of vascular cell proliferation,[11] and enhancement of oxidative stress by iron-catalyzed hydroxyl radical formation via Fenton chemistry and subsequent lipid peroxidation.[12]

See page 2235

In previous studies, we have reported that long-term administration of angiotensin II (Ang II) in rats caused accumulation of iron in the kidney,[13,14] heart,[15] and liver,[16] and that this may play a role in regulating the gene expression and function in these organs. Thus far, little is known about whether Ang II induces aberrant iron homeostasis in the vascular tissue; however, if so, it might exacerbate the oxidant-induced vascular damage initiated by increased production of superoxide[17] generated by activated NAD(P)H oxidase.[18] In this context, it may be of note that iron chelation decreased the extent of in vivo oxidative stress in animals with long-term Ang II infusion.[19,20]

In the present study, we have investigated the extent of iron accumulation and ferritin induction in the aortas of Ang II-infused animals, and the possible relationship between these phenomena, modulation of gene expression, and vascular function and remodeling.

Methods

Animal Models

The experiments were performed in accordance with the guidelines for animal experimentation approved by the Animal Center for

Original received February 17, 2005; final version accepted July 25, 2005.

From the Department of Cardiovascular Medicine (N.I., K.S., G.M., M.O., R.N.), University of Tokyo Graduate School of Medicine, and the Department of Pathology, Wakayama Medical College (I.M.), Japan.

Correspondence to Dr Nobukazu Ishizaka, Department of Cardiovascular Medicine, University of Tokyo, Graduate School of Medicine, Hongo 7-3-1, Bunkyo-ku, Tokyo 113-8655, Japan. E-mail nobuishizka-tky@umin.ac.jp

Arterioscler Thromb Vasc Biol. is available at http://www.atvbaha.org DOI: 10.1161/01.ATV.0000181763.57495.2b

Biomedical Research, Faculty of Medicine, University of Tokyo. Ang II-induced hypertension was induced in male Sprague-Dawley rats by subcutaneous implantation of an osmotic minipump (Alzet model 2001; Alza Pharmaceutical, Palo Alto, Calif) as described previously.[21] Briefly, Val^5–Ang II (Sigma Chemical, St Louis, Mo) was infused at a dose of 0.7 mg/kg per day for 7 days, which significantly increased the blood pressure of rats (192±4 mm Hg, n=10, $P<0.01$ versus control rats, 131±3 mm Hg, n=6). To contrast this model with another model of hypertension, norepinephrine (Sigma Chemical) was infused at a rate of 2.8 mg/kg per day, which resulted in a comparable hypertensive effects (196±6 mm Hg, n=9) to those of Ang II.[21] Ang II was infused 0.7 mg/kg per day in the current experiments unless stated otherwise. Subpressor dose of Ang II was a dose of 0.25 mg/kg per day, which did not significantly increase the systolic blood pressure of rats as compared with untreated rats (134±3 mm Hg, n=6).

Iron chelator, deferoxamine (a kind gift from Novartis) was subcutaneously administered at a dose of 200 mg/kg per day, which did not significantly affect the blood pressure of Ang II-infused rats (196±7 mm Hg, n=9). Iron-overload was achieved by 4 intraperitoneal injections of an iron–dextran complex (a kind gift from Teikoku Hormone Mfg, Tokyo, Japan) at a dose of 240 mg of elemental iron/kg, which did not significantly alter the blood pressure (131±3 mm Hg, n=10) compared with untreated control.

Protein Purification and Western Blot Analysis

Protein was isolated by homogenizing samples in the lysis buffer containing protease inhibitors as described previously.[21] Polyclonal antibodies against rat ferritin (Panapharm, Kumamoto, Japan) and heme oxygenase-1 (HO-1) (StressGen, Victoria, BC, Canada), and monoclonal antibody against β-actin (Sigma) and 4-hydroxynonenal (HNE)-modified protein (NOF, Tokyo, Japan) were used at dilutions of 1/1000, 1/2000, 1/2000, and 1/3000, respectively.[15] The ECL Western blotting system (Amersham Life Sciences, Arlington Heights, Ill) was used for detection. Bands were visualized by a lumino-analyzer (Fuji Photo Film, Tokyo, Japan). Band intensity was calculated and is expressed as a percentage of the control value.

Histological and Immunohistochemical Analyses

For histological and immunohistochemical analyses, formalin-fixed paraffin-embedded specimen was used except in the cases of staining for HNE-modified proteins and for monocyte chemoattractant protein-1 (MCP-1), in which Bouin-fixed paraffin-embedded specimen and unfixed frozen sections, respectively, were used. Immunohistochemistry was performed as described previously.[15] Primary antibodies against rat macrophage/monocyte (ED-1; Chemicon International, Temecula, Calif), human α-smooth muscle actin (Sigma Chemical), rat ferritin, HNE-modified proteins, and rat MCP-1 (IBL, Gunma, Japan) were used at dilutions of 1/200, 1/1,000, 1/200, 1/50, and 1/100, respectively. In some immunohistochemical studies, relevant pre-immune IgG controls were used as control antibodies. For immunofluorescence staining, rhodamine-conjugated anti-mouse (Chemicon International) and fluorescein-conjugated anti-rabbit (Sigma Chemical) antibodies were used at a dilution of 1/100. Laser scanning confocal fluorescence microscopy combined with differential interference contrast imaging was performed using FLUOVIEW FV300 (Olympus, Tokyo, Japan). Tissue iron content was analyzed with atomic absorption spectrophotometry.

Isolated Vascular Ring Experiments

Ring segments (5 mm in length) of the thoracic aorta were suspended in individual organ chambers filled with Krebs buffer of the following composition (mmol/L): NaCl, 118.3; KCl, 4.7; $CaCl_2$, 2.5; $MgSO_4$, 1.2; KH_2PO_4, 1.2; $NaHCO_3$, 25.0; and glucose, 10, pH 7.4. The solution was continuously aerated with a 95% O_2, 5% CO_2 mixture, which was maintained at 37°C. Isometric tension was recorded by using an isometric force displacement transducer (NIHON KOHDEN, Tokyo, Japan) connected to a data acquisition system (Power Laboratory Chart 5; AD Instruments, Colo). The vessels were then precontracted with phenylephrine (3×10^{-6} mol/L). After a stable contraction plateau was reached, the rings were exposed to either acetylcholine or sodium nitroprusside (SNP).

RNA Extraction, Northern Blot Analysis, and Real-Time Reverse-Transcription Polymerase Chain Reaction

Total RNA was isolated from homogenized aorta by the acid guanidinium thiocyanate-phenol chloroform method as described previously.[22] Probes were obtained by polymerase chain reaction (PCR) with reverse-transcription using the primers 5′-CAGGTCTCTGTCACGCTTCT-3′ and 5′-AGTATTCATGGAAGGGAATAG-3′ for MCP-1. The reverse-transcription PCR product was subcloned into a p-GEM-T vector (Promega, Madison, Wis), and the cDNA was confirmed as rat MCP-1 by direct sequencing. For Northern blotting, a rat MCP-1 cDNA probe was labeled with [α-32P]-dCTP by a DNA labeling kit (Nippon Gene, Tokyo, Japan), and hybridized at 42°C overnight.

To investigate the mRNA expression of transferrin receptor, H-ferritin, and L-ferritin, real-time quantitative PCR with gene-specific hybriprobes was performed by LightCycler (Roche Diagnostics, Basel, Switzerland) after first-strand cDNA was synthesized with 2 μg of total RNA as a template using a SuperScript First-Strand Synthesis System (Invitrogen, Carlsbad, Calif). The used primer sets were as follows: Transferrin receptor, sense primer, 5′-GGA GAC TAC TTC CGT GCT ACT T-3′, antisense primer, 5′-AGA GCC CCA GAA GAT GTG TC-3′; H-ferritin, sense primer, 5′- CAA ACT GGC TAC TGA CAA GAA T-3′ antisense primer, 5′- TGGAGCGCATCCACTTGA-3′; L-ferritin, sense primer, 5′-AAG TGG AAG CTG CCG TGA A-3′, antisense primer, 5′-CTG CAA CTT GAG GAG ACG C-3′. The mRNA expression of these genes were normalized to GAPDH mRNA expression, which was also assessed by the real-time PCR with sense primer 5′-TGA ACG GGA AGC trichloroacetic acid CTG G-3′, and antisense primer 5′= TCC ACC ACC CTG TTG CTG TA-3′ and presented as the percentages of the data from aortas of untreated animals.

Remodeling of Aortic Wall

The degree of vascular remodeling (the medial thickness and perivascular fibrosis) was estimated in the aortas of the rat subjected Ang II administration at a dose of 0.7 mg/kg per day for 28 days. Some rats were given subcutaneous infusion of deferoxamine at a dose of 200 mg/kg per day for the last 14 days. Aortas were perfused with physiological saline solution and fixed with 6% formaldehyde solution for 30 minutes via infusion into the left ventricle at a pressure of 90 mm Hg. Thoracic aorta was cut into six pieces after excised. The paraffin-embedded specimens in the 2 mm of thickness were stained with hematoxylin and eosin and Masson's trichrome staining. To evaluated vascular wall thickness, the wall-to-lumen ratio of the aorta was examined, and for perivascular fibrosis, fibrosis area was measured as described previously[15,23] and calculated as perivascular fibrosis surrounding the vessel wall to the vessel area. Histopathology and morphometry were performed by investigators who were unaware of the treatment being administered.

Statistical Analysis

Data are expressed as the mean±SEM. We used ANOVA followed by a multiple comparison test to compare raw data, before expressing the results as a percentage of the control value using the statistical analysis software Statistica version 5.1 J for Windows (StatSoft Inc, Tulsa, Okla). A value of $P<0.05$ was considered to be statistically significant

Results

Treatment of Ang II, Norepinephrine, Deferoxamine, and Iron Dextran on Aortic Expression of Ferritin and HO-1

Administration of pressor dose Ang II for 7 days increased aortic ferritin expression ≈25-fold over control values. Non-

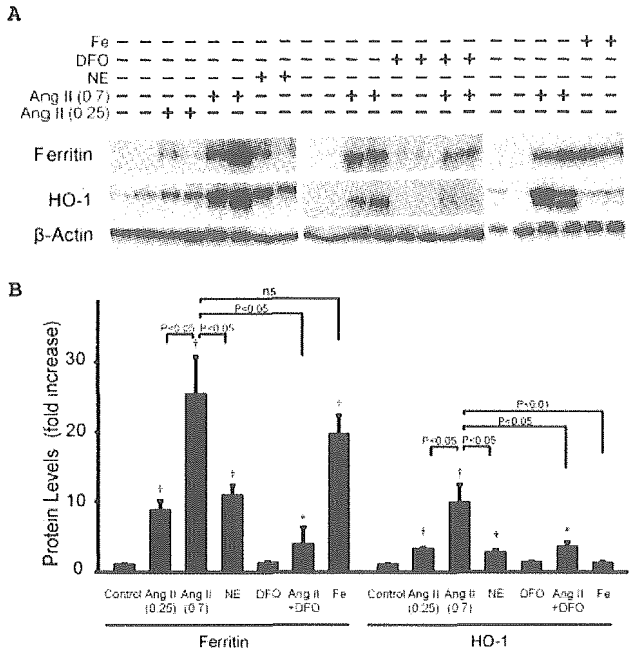

Figure 1. Expression of ferritin and heme oxygenase-1 (HO-1) in the aortas of rats treated with angiotensin II (Ang II), deferoxamine (DFO), and iron dextran (Fe). For Ang II administration, 2 doses were used; 0.7 mg/kg per day (pressor dose), and 0.25 mg/kg per day (nonpressor dose). A, Representative Western blots. B, Summary of the data from 4 to 6 experiments for each group. *$P<0.05$ and †$P<0.01$ vs untreated control.

pressor dose Ang II and pressor dose of norepinephrine also increased aortic ferritin expression, although to a significantly lesser extent (Figure 1). The pattern of regulation of HO-1 by these Ang II and norepinephrine was similar to that of ferritin. Treatment of Ang II-infused rats with deferoxamine partially suppressed upregulation of ferritin and HO-1. Iron overload achieved by the administration of iron dextran, which increases the serum iron levels ≈90-fold over control values,[24] caused induction of ferritin to a similar extent as Ang II; however, it did not significantly increase aortic HO-1 expression (Figure 1).

Localization of Ferritin and Iron Deposition

Immunohistochemical analysis showed that ferritin was expressed mainly in the aortic endothelial cells and only weakly in the adventitial cells in untreated control rats, and ferritin expression appeared to be enhanced after Ang II infusion (Figure 2A through 2F). Confocal microscopy showed that some of the ferritin-positive cells were also positive for ED-1, thus monocytes/macrophages (Figure 2G). Iron was not histologically evident by Prussian blue staining in the aorta of untreated rats (Figure 2H). After 7 days of Ang II infusion, some of the adventitial cells were found to be positive for iron, although stainable iron was not evident in the endothelium (Figure 2I). No apparent iron deposition could be observed in the aortas of rats treated with both Ang II and an iron chelator (Figure 2J). In the aortas of rats treated with iron dextran, iron deposition could be observed both in the adventitial and endothelial cells (Figure 2K). Staining of serial sections showed that iron positive cells in the adventitial layer were

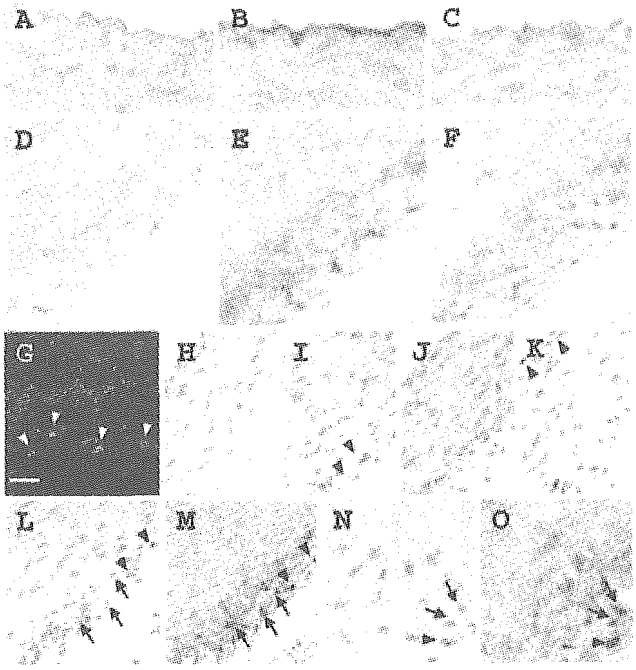

Figure 2. Expression of ferritin protein and deposition of iron in the aortas from untreated and Ang II-treated animals. Sections are from the aortas of untreated rats (A, D, H), rats treated with Ang II (B, C, E, F, G, I, L–O), from rats treated with Ang II and deferoxamine (J), and from rats treated with iron dextran (K). B, C, E, F, L, M, N, O, Serial specimens. A, B, D, E, Ferritin staining of the aortas from untreated (A, D) and Ang II-treated (B, D) animals. There was a weak ferritin expression in the vascular endothelial (A) and adventitial (C) cells in the aortas of untreated rats. After Ang II treatment, intensity of ferritin staining increased (B, D). In G, red and green signals indicate ferritin and ED-1-positivity, respectively. C and F, Immunohistochemistry using pre-immune rabbit IgG as a primary antibody that showed no apparent staining. Some of the ferritin-positive cells in the adventitial layer stained positively for ED-1 (G, arrowheads). No iron-positive cells were observed in the aortas from untreated rats (H). Positive iron staining could be observed in the cells in the adventitial layer in the aortas from Ang II-infused rats (I, arrowheads), but not in those from rats treated with both Ang II and deferoxamine (J). In rats subjected to iron overload, iron staining was positive in the endothelial (arrowheads) and adventitial cells (K). Adventitial cells that were positive for iron were positive for ferritin staining, but only a fraction of ferritin-positive cells were positive for iron (L, M, arrowheads), and some of the ferritin-positive cells were negative for iron staining (L, M, arrows). Iron positive-adventitial cells were positive for ED-1 (N, O, arrowheads), thus judged to be monocytes/macrophages. There are some ED-1–positive cells that were negative for iron staining (N, O, arrows). Scale bar, 20 μm (G). Original magnifications, ×200 (H–M), ×400 (A–F, N, O).

positive for ferritin (Figure 2L and 2M). Of ferritin-positive adventitial cells, 7.4±2.0% of such cells were found to be positive for stainable iron (number of rats=6). Iron-positive adventitial cells were also positive for ED-1 (Figure 2N and 2O), thus they were judged to be monocytes/macrophages.

Tissue iron content in the aortas in the untreated animals were 58.1±3.0 μg/g dry weight (n=4). Ang II treatment significantly increased the aortic iron content (121.7±19.8 μg/g dry weight, n=9, $P<0.05$ versus untreated control), which was reversed by the treatment with deferoxamine

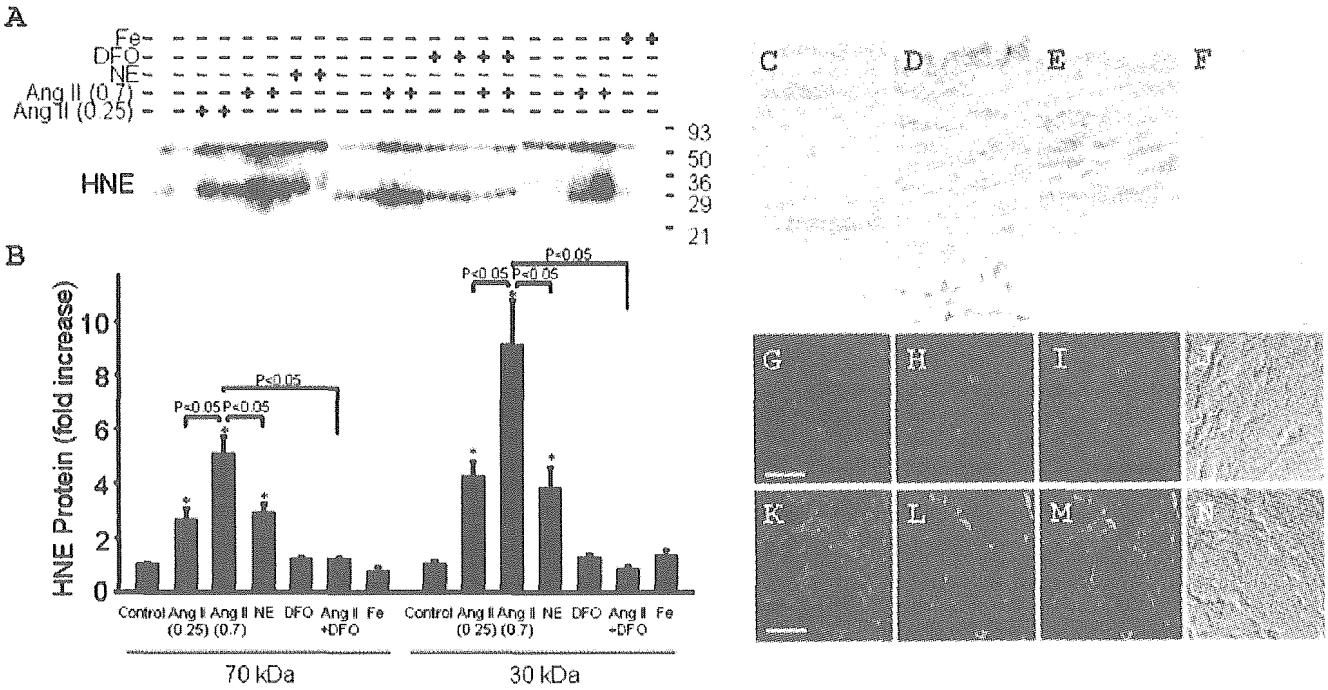

Figure 3. Expression and localization of HNE protein adducts and ferritin. A and B, Western blot analysis. A, Representative Western blot. B, Summary of the data from 4 to 6 experiments for each group. *$P<0.01$ vs untreated control. C–N, Immunohistochemistry. Sections are from the aortas of untreated rats (C, G–J), rats treated with Ang II (D, F, K–N), and from rats treated with Ang II and deferoxamine (E). C–E, Staining for HNE-protein, visualized by 3,3-diaminobenzidine tetrahydrochloride. Aortas from untreated (A), angiotensin II (Ang II)-treated, and Ang II plus deferoxamine-treated rats (C) are shown. Increased staining for HNE-modified protein was observed in the endothelial cells and adventitial cells (arrows) in the aortas from Ang II-infused animals. F, Pre-immune mouse IgG was used in the place of primary antibody. G–N, Confocal microscopic observation (G–I, K–M) and differential interference contrast imaging (J, N). Pictures from the same sections are shown in G–J and K–N. G and K, Ferritin staining. H and L, Staining for HNE-modified proteins. I and M. Merge. Some ferritin-positive cells were also positive for HNE-modified proteins (J). Original magnifications, ×200 (C–F). Scale bar, 20 μm (G, K).

(n=4) (Ang II plus deferoxamine, 52.6±5.3 μg/g dry weight, P=nonsignificant versus untreated control).

Localization and Expression of HNE-Modified Proteins

We next examined the expression HNE-modified protein adducts, markers of lipid peroxidation. Western blot analysis showed that a major band of HNE-protein adducts could be observed mainly at sizes of ≈30 and 70 kDa, and intensity of both of these bands were robustly increased after Ang II infusion (Figure 3A and 3B). Subpressor dose Ang II and norepinephrine also increased the amount of HNE-modified proteins, although to significantly lesser extent than pressor dose Ang II. Chelation of iron suppressed the increase in HNE-modified proteins induced by Ang II. Iron dextran treatment did not significantly alter the expression of HNE-modified proteins.

We then examined the distribution of HNE-modified protein adducts by immunohistochemistry. In the aortas of untreated rat, expression of HNE-modified proteins was observed weakly in all layers of the aorta (Figure 3C). After Ang II infusion, staining of HNE-modified proteins was more intense especially in the endothelial and adventitial cells (Figure 3D). This Ang II-induced increase was reversed by the concomitant administration of deferoxamine (Figure 3E). Confocal microscopy showed that the adventitial cells with increased HNE-modified protein adducts were positive for ferritin (Figure 3G through 3N).

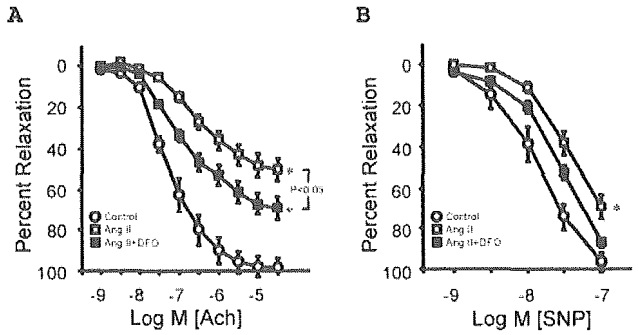

Figure 4. Relaxation in aortic rings induced by acetylcholine and sodium nitroprusside. A, Relaxation to acetylcholine. B, Relaxation to sodium nitroprusside. Open circles, open squares, and closed squares indicate aortas from untreated (n=8), angiotensin II (Ang II)-treated (n=8), and Ang II + deferoxamine (DFO)-treated (n=10) rats, respectively. *$P<0.01$ vs untreated control.

Relaxations of Aortic Segments

Peak relaxation produced by acetylcholine in aortas from Ang II-treated animals (50.4±5.7%, n=8) was significantly reduced compared with untreated rats (98.5±5.1%, n=8). Treatment with deferoxamine reversed, although only partially, the impaired vascular relaxation in response to acetylcholine in Ang II-treated animals (69.2±6.0%, n=10) (Figure 4A). Ang II treatment also blunted peak relaxation

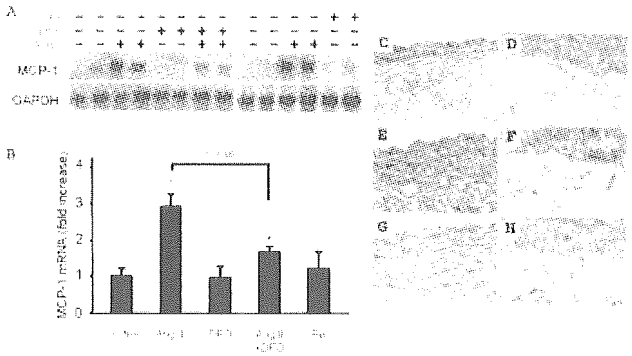

Figure 5. Expression and localization of MCP-1 in the aortas of rats treated with angiotensin II (Ang II). A and B, Western blot analysis. A, Representative Western blot. B, Summary of the data from 4 to 6 experiments for each group. *$P<0.05$ and †$P<0.01$ vs untreated control. C–H, Immunohistochemistry. Sections are from the aortas of untreated rats (C, D), and rats treated with Ang II (E–H). C–F, Staining for MCP-1-protein, visualized by 3,3-diaminobenzidine tetrahydrochloride. Increased staining for MCP-1 was observed in medial layer smooth muscle cells in the aortas from Ang II-infused animals. G and H. Pre-immune rabbit IgG was used in the place of primary antibody.

induced by SNP, which was again suppressed by the deferoxamine treatment (Figure 4B).

Effects of Chelation of Iron in the Ang II-Induced Upregulation of MCP-1 in the Aorta

We showed previously that Ang II increases the expression of the MCP-1 in rat aorta.[25] Here we examined the effects of iron chelation on Ang II-induced aortic MCP-1 upregulation. Ang II increased aortic expression ≈3-fold over control, which was partially suppressed by treatment with deferoxamine (Figure 5). However, iron dextran did not significantly affect MCP-1 expression. Then localization of MCP-1 was investigated using antibody against rat MCP-1. As shown in Figure 5C through 5H, expression of MCP-1 protein was increased mainly in the medial layer smooth muscle cells in the aortas of Ang II-infused animals.

Effect of Iron Chelation on Ang II-Induced Remodeling of Aortic Wall

We next examined whether deferoxamine have any effects on Ang II-induced vascular remodeling. For this purpose, Ang II was administered for 28 days, and some rats were given deferoxamine for 14 consecutive days starting 14 days after the initiation of Ang II infusion. Systolic blood pressure of rats received Ang II alone and Ang II plus deferoxamine were 196±11 mm Hg and 196±6 mm Hg, respectively (P=nonsignificant). Compared with untreated control, Ang II infusion significantly increased the wall-to-lumen ratio from 0.22±0.01 (n=6) to 0.39±0.01 (n=8) ($P<0.0001$), which was partially suppressed by concomitant administration of DFO (0.35±0.01, n=10, $P<0.001$ versus control and $P<0.01$ versus Ang II-infused animals). Ang II infusion also increased the area of perivascular fibrosis compared with untreated control (control, 0.11±0.01 [n=6]; Ang II 0.23±0.012 [n=8], $P<0.001$), and these increases were again in part inhibited by the deferoxamine treatment (0.16±0.01, n=10, $P<0.01$ versus control, and $P<0.01$ versus Ang II-infused animals) (Figure 6).

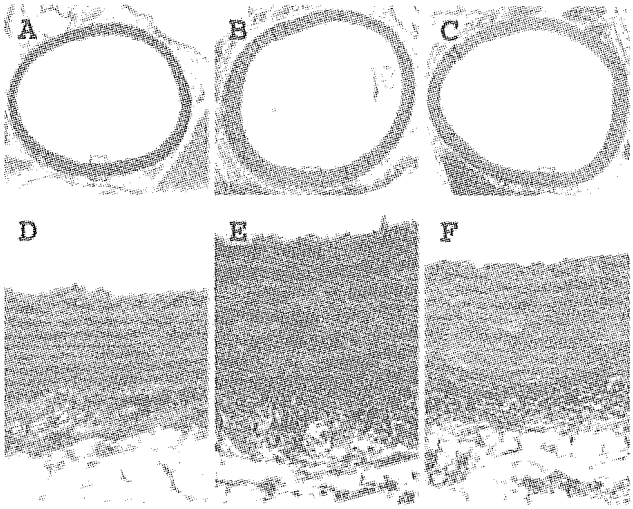

Figure 6. Inhibition of Ang II-induced vascular remodeling by deferoxamine. Masson trichrome staining of the aortas of the untreated (A, D), Ang II-treated (B, D), and Ang II plus deferoxamine-treated rats (C, F) are shown. D, E, and F are higher-magnification images of bracketed region of A, B, and C, respectively. Original magnifications, ×100 (A–C), ×400 (D–F).

Expression of Transferrin Receptor, H-ferritin, and L-ferritin

Finally, we evaluated whether mRNA levels of transferrin receptor, H-ferritin, and L-ferritin were regulated in the aortas of Ang II-infused animals. Compared with the aortas of untreated-animals (n=15) (transferrin receptor 100±18%; H-ferritin 100±12%; L-ferritin 100±7%), mRNA expression of all these tested genes in the aortas of Ang II-infused animals (n=13) were found to be significantly greater (transferrin receptor 313±50%, $P<0.0001$; H-ferritin 137±15%, $P<0.05$; L-ferritin 161±17%, $P<0.01$).

Discussion

In the present study, we have demonstrated that long-term administration of Ang II caused upregulation of ferritin expression and deposition of iron in the aortic wall of rats. Ang II also increased the expression of oxidative stress markers, HO-1 and HNE-modified proteins. Chelation of iron partially suppressed Ang II-induced upregulation of ferritin, HO-1, and HNE-modified proteins. In addition, iron chelation also partially reversed the impaired vascular relaxation in response to acetylcholine and SNP, and upregulation of MCP-1 mRNA induced by Ang II. These data collectively suggest that changes in iron homeostasis may in part contribute to the regulation of aortic gene expression and alteration of vascular function induced by long-term administration of Ang II.

Increased ferritin expression in the vasculature and its potential physiological importance have been demonstrated in several previous articles. Pang et al have reported that ferritin expression was increased in atherosclerotic aortas from animals and humans compared with nonatherosclerotic counterparts.[3] Interestingly, there are some similar histolog-

ical and immunohistological findings between in the early atherosclerotic lesions reported in Pang et al's study and in the aortas of Ang II-infused animals in the present investigation, namely an increased expression of ferritin was observed in the endothelial cells and macrophages.[3] In addition, this group and others also reported that expression of HO-1 was increased in the endothelial cells and macrophages in the atherosclerotic lesions,[26,27] and we also found that expression of HO-1 was upregulated in the aortas of Ang II-infused animals in both a previous report[21] and the current one. In addition, Lee et al have demonstrated a close association between iron deposition and the progression of atherosclerosis in the atherosclerosis-prone animal models, and have noted that restriction of iron intake inhibited lesion formation in these animals.[9] In the current study, Ang II upregulated aortic expression of MCP-1, a chemokine that is postulated to play a central role in vascular damage and atherogenesis,[28] and this was inhibited by iron chelation may support this notion. From these observations, it seems possible that ferritin induction and iron accumulation in the aortic wall may have a role in potentiating the pro-atherogenic properties of Ang II.

In the present study, iron chelation, although partially, suppressed the Ang II-induced impaired vascular relaxation in response to acetylcholine and SNP. This finding suggests that altered ferritin induction and/or iron deposition may have a role in modulating vascular function in Ang II-infused animals. It is noteworthy that effects of iron chelation in preventing vascular dysfunction in some diseased conditions, such as diabetes, have also been reported in some previous articles.[12,29] Acetylcholine-induced vascular relaxation has also been shown to be significantly attenuated by hydroxyl radicals generated by Fenton reagents.[30] These findings may collectively support the notion that the effects of iron chelation in attenuating Ang II-induced vascular dysfunction may relate to a reduction in the extent of oxidative stress, presumably a function of iron-catalyzed generation of hydroxyl radicals via Fenton chemistry.

We also found that deferoxamine inhibited arterial remodeling, that is the medial thickening and perivascular fibrosis, in the aortas of rats receiving Ang II infusion for 4 weeks. It has been reported recently that iron chelation, as well as adenovirus-mediated introduction of catalase decreased the extent of cardiac hypertrophy induced by serotonin.[31] In addition, hypertrophic effects of glycosylated oxyhemoglobin on vascular smooth muscle cells could be suppressed by deferoxamine, as well as superoxide dismutase and catalase.[32] These data suggest that iron may play a crucial role in the development of hypertrophy of cardiovascular system through reducing the production of toxic oxygen free radicals. Recent studies also suggested that iron and/or iron-mediated increase in the extent of oxidative stress play a role in the fibrotic changes not only in the liver[16,33] but also in other organs such as heart.[34,35] Our data may suggest the possibility that iron may also have a role in the vascular remodeling in vivo in certain diseased conditions, such as increased circulating Ang II.

We demonstrated that Ang II infusion increased the expression of 2 oxidative stress markers, HO-1[36] and HNE-modified proteins, and both were suppressed by iron chelation. Although these data are compatible to the notion that deferoxamine reduced the extent of oxidative stress induced by Ang II, one has to be also aware of the possible alternative scenario that deferoxamine may have directly reduced HO-1 expression by inducing Bach1, a heme-regulated transcriptional repressor for HO-1.[37]

In the current study, we showed that Ang II increased the ferritin expression and iron content of the aorta and that aortic expression of transferrin receptor was increased. Intracellular iron content may be affected by the transferrin receptor-mediated uptake of iron. It has been reported that exposure of vascular cells as well as fibroblasts to hydrogen peroxide increased the expression of transferrin receptor.[38,39] Ang II stimulation may result in an enhancement of the degree of oxidative stress by activating membrane NADH oxidase,[18] and in an increase in the hydrogen peroxide concentration of vascular cells.[40] Thus, it is possible that increased oxidative stress evoked by Ang II induced aortic expression transferrin receptor, which resulted in increased aortic iron content. Until now, the expression and regulation of several genes related to iron metabolism,[41] such as divalent metal transporter-1, ferroportin-1, and hephaestin, are yet to be fully understood in the vascular cells; therefore, whether expression of these genes are affected by Ang II in the vessel wall should be clarified in future studies.

In summary, long-term administration of Ang II induced the upregulation of ferritin and deposition of iron in the aortic wall. Iron chelation attenuated the induced increase in the expression of oxidative stress markers, HO-1 and 4-HNE-modified proteins, in the aortic wall, as well as Ang II-induced MCP-1 mRNA upregulation and impairment of vascular responsiveness to acetylcholine and exogenous form of nitric oxide induced by Ang II. Taken together, these data suggest that aberrant iron homeostasis may have a role in the Ang II-induced regulation of pro-atherogenic gene expression, vascular function, and vascular remodeling.

Acknowledgments

This work was supported by Grants-in-Aid for Scientific Research from the Ministry of Education, Science, and Culture of Japan (Grant 13671098), grants from Novartis Foundation for Gerontological Research, and that from Takeda Medical Research Foundation. We thank Kyoko Furuta, Kazuko Komatsumoto, and Naoko Amitani for their excellent technical assistance.

References

1. Swain J, Gutteridge JM. Prooxidant iron and copper, with ferroxidase and xanthine oxidase activities in human atherosclerotic material. *FEBS Lett.* 1995;368:513–515.
2. Yuan XM, Anders WL, Olsson AG, Brunk UT. Iron in human atheroma and LDL oxidation by macrophages following erythrophagocytosis. *Atherosclerosis.* 1996;124:61–73.
3. Pang JH, Jiang MJ, Chen YL, Wang FW, Wang DL, Chu SH, Chau LY. Increased ferritin gene expression in atherosclerotic lesions. *J Clin Invest.* 1996;97:2204–2212.
4. Lee FY, Lee TS, Pan CC, Huang AL, Chau LY. Colocalization of iron and ceroid in human atherosclerotic lesions. *Atherosclerosis.* 1998;138:281–288.
5. Lee TS, Lee FY, Pang JH, Chau LY. Erythrophagocytosis and iron deposition in atherosclerotic lesions. *Chin J Physiol.* 1999;42:17–23.
6. Nitenberg A, Paycha F, Ledoux S, Sachs R, Attali JR, Valensi P. Coronary artery responses to physiological stimuli are improved by def-

eroxamine but not by L-arginine in non-insulin-dependent diabetic patients with angiographically normal coronary arteries and no other risk factors. *Circulation.* 1998;97:736–743.
7. Duffy SJ, Biegelsen ES, Holbrook M, Russell JD, Gokce N, Keaney JF Jr, Vita JA. Iron chelation improves endothelial function in patients with coronary artery disease. *Circulation.* 2001;103:2799–2804.
8. Matthews AJ, Vercellotti GM, Menchaca HJ, Bloch PH, Michalek VN, Marker PH, Murar J, Buchwald H. Iron and atherosclerosis: inhibition by the iron chelator deferiprone (L1). *J Surg Res.* 1997;73:35–40.
9. Lee TS, Shiao MS, Pan CC, Chau LY. Iron-deficient diet reduces atherosclerotic lesions in apoE-deficient mice. *Circulation.* 1999;99: 1222–1229.
10. Pratico D, Pasin M, Barry OP, Ghiselli A, Sabatino G, Iuliano L, FitzGerald GA, Violi F. Iron-dependent human platelet activation and hydroxyl radical formation: involvement of protein kinase C. *Circulation.* 1999;99:3118–3124.
11. Porreca E, Ucchino S, Di Febbo C, Di Bartolomeo N, Angelucci D, Napolitano AM, Mezzetti A, Cuccurullo F. Antiproliferative effect of desferrioxamine on vascular smooth muscle cells in vitro and in vivo. *Arterioscler Thromb.* 1994;14:299–304.
12. Pieper GM, Siebeneich W. Diabetes-induced endothelial dysfunction is prevented by long-term treatment with the modified iron chelator, hydroxyethyl starch conjugated-deferoxamine. *J Cardiovasc Pharmacol.* 1997;30:734–738.
13. Ishizaka N, Aizawa T, Yamazaki I, Usui S, Mori I, Kurokawa K, Tang SS, Ingelfinger JR, Ohno M, Nagai R. Abnormal iron deposition in renal cells in the rat with chronic angiotensin II administration. *Lab Invest.* 2002;82:87–96.
14. Saito K, Ishizaka N, Aizawa T, Sata M, Iso ON, Noiri E, Ohno M, Nagai R. Role of aberrant iron homeostasis in the upregulation of transforming growth factor-beta1 in the kidney of angiotensin II-induced hypertensive rats. *Hypertens Res.* 2004;27:599–607.
15. Ishizaka N, Saito K, Mitani H, Yamazaki I, Sata M, Usui S, Mori I, Ohno M, Nagai R. Iron overload augments angiotensin II-induced cardiac fibrosis and promotes neointima formation. *Circulation.* 2002;106: 1840–1846.
16. Ishizaka N, Saito K, Noiri E, Sata M, Ikeda H, Ohno A, Ando J, Mori I, Ohno M, Nagai R. Administration of ANG II induces iron deposition and upregulation of TGF-beta1 mRNA in the rat liver. *Am J Physiol Regul Integr Comp Physiol.* 2005;288:R1063–R1070.
17. Kvietys PR, Inauen W, Bacon BR, Grisham MB. Xanthine oxidase-induced injury to endothelium: role of intracellular iron and hydroxyl radical. *Am J Physiol.* 1989;257:H1640–H1646.
18. Fukui T, Ishizaka N, Rajagopalan S, Laursen JB, Capers QT, Taylor WR, Harrison DG, de Leon H, Wilcox JN, Griendling KK. p22phox mRNA expression and NADPH oxidase activity are increased in aortas from hypertensive rats. *Circ Res.* 1997;80:45–51.
19. Aizawa T, Ishizaka N, Usui S, Ohashi N, Ohno M, Nagai R. Angiotensin II and catecholamines increase plasma levels of 8-epi-prostaglandin F(2alpha) with different pressor dependencies in rats. *Hypertension.* 2002;39:149–154.
20. Saito K, Ishizaka N, Mitani H, Ohno M, Nagai R. Iron chelation and a free radical scavenger suppress angiotensin II-induced downregulation of klotho, an anti-aging gene, in rat. *FEBS Lett.* 2003;551:58–62.
21. Ishizaka N, de Leon H, Laursen JB, Fukui T, Wilcox JN, De Keulenaer G, Griendling KK, Alexander RW. Angiotensin II-induced hypertension increases heme oxygenase-1 expression in rat aorta. *Circulation.* 1997; 96:1923–1929.
22. Aizawa T, Ishizaka N, Taguchi J, Nagai R, Mori I, Tang SS, Ingelfinger JR, Ohno M. Heme oxygenase-1 is upregulated in the kidney of angiotensin II-induced hypertensive rats: possible role in renoprotection. *Hypertension.* 2000;35:800–806.
23. Ishizaka N, Aizawa T, Mori I, Taguchi J, Yazaki Y, Nagai R, Ohno M. Heme oxygenase-1 is upregulated in the rat heart in response to chronic administration of angiotensin II. *Am J Physiol Heart Circ Physiol.* 2000; 279:H672–H678.
24. Ishizaka N, Saito K, Noiri E, Sata M, Mori I, Ohno M, Nagai R. Iron dextran causes renal iron deposition but not renal dysfunction in angiotensin II-treated and untreated rats. *Nephron Physiol.* 2004;98:107–113.
25. Capers QT, Alexander RW, Lou P, De Leon H, Wilcox JN, Ishizaka N, Howard AB, Taylor WR. Monocyte chemoattractant protein-1 expression in aortic tissues of hypertensive rats. *Hypertension.* 1997;30:1397–1402.
26. Wang LJ, Lee TS, Lee FY, Pai RC, Chau LY. Expression of heme oxygenase-1 in atherosclerotic lesions. *Am J Pathol.* 1998;152:711–720.
27. Nakayama M, Takahashi K, Komaru T, Fukuchi M, Shioiri H, Sato K, Kitamuro T, Shirato K, Yamaguchi T, Suematsu M, Shibahara S. Increased expression of heme oxygenase-1 and bilirubin accumulation in foam cells of rabbit atherosclerotic lesions. *Arterioscler Thromb Vasc Biol.* 2001;21:1373–1377.
28. Egashira K. Molecular mechanisms mediating inflammation in vascular disease: special reference to monocyte chemoattractant protein-1. *Hypertension.* 2003;41:834–841.
29. Coppey LJ, Gellett JS, Davidson EP, Dunlap JA, Lund DD, Yorek MA. Effect of antioxidant treatment of streptozotocin-induced diabetic rats on endoneurial blood flow, motor nerve conduction velocity, and vascular reactivity of epineurial arterioles of the sciatic nerve. *Diabetes.* 2001;50: 1927–1937.
30. Todoki K, Okabe E, Kiyose T, Sekishita T, Ito H. Oxygen free radical-mediated selective endothelial dysfunction in isolated coronary artery. *Am J Physiol.* 1992;262:H806–H812.
31. Bianchi P, Pimentel DR, Murphy MP, Colucci WS, Parini A. A new hypertrophic mechanism of serotonin in cardiac myocytes: receptor-independent ROS generation. *FASEB J.* 2005;19:641–643.
32. Peiro C, Angulo J, Rodriguez-Manas L, Llergo JL, Vallejo S, Cercas E, Sanchez-Ferrer CF. Vascular smooth muscle cell hypertrophy induced by glycosylated human oxyhaemoglobin. *Br J Pharmacol.* 1998;125: 637–644.
33. Templeton DM, Liu Y. Genetic regulation of cell function in response to iron overload or chelation. *Biochim Biophys Acta.* 2003;1619:113–124.
34. Carthew P, Smith AG, Hider RC, Dorman B, Edwards RE, Francis JE. Potentiation of iron accumulation in cardiac myocytes during the treatment of iron overload in gerbils with the hydroxypyridinone iron chelator CP94. *Biometals.* 1994;7:267–271.
35. Saito K, Ishizaka N, Aizawa T, Sata M, Iso-o N, Noiri E, Mori I, Ohno M, Nagai R. Iron chelation and a free radical scavenger suppress angiotensin II-induced upregulation of TGF-beta1 in the heart. *Am J Physiol Heart Circ Physiol.* 2005;288:H1836–H1843.
36. Ryter SW, Choi AM. Heme oxygenase-1: molecular mechanisms of gene expression in oxygen-related stress. *Antioxid Redox Signal.* 2002;4: 625–632.
37. Kitamuro T, Takahashi K, Ogawa K, Udono-Fujimori R, Takeda K, Furuyama K, Nakayama M, Sun J, Fujita H, Hida W, Hattori T, Shirato K, Igarashi K, Shibahara S. Bach1 functions as a hypoxia-inducible repressor for the heme oxygenase-1 gene in human cells. *J Biol Chem.* 2003;278:9125–9133.
38. Pantopoulos K, Hentze MW. Rapid responses to oxidative stress mediated by iron regulatory protein. *EMBO J.* 1995;14:2917–2924.
39. Tampo Y, Kotamraju S, Chitambar CR, Kalivendi SV, Keszler A, Joseph J, Kalyanaraman B. Oxidative stress-induced iron signaling is responsible for peroxide-dependent oxidation of dichlorodihydrofluorescein in endothelial cells: role of transferrin receptor-dependent iron uptake in apoptosis. *Circ Res.* 2003;92:56–63.
40. Zafari AM, Ushio-Fukai M, Akers M, Yin Q, Shah A, Harrison DG, Taylor WR, Griendling KK. Role of NADH/NADPH oxidase-derived H2O2 in angiotensin II-induced vascular hypertrophy. *Hypertension.* 1998;32:488–495.
41. Andrews NC. Iron homeostasis: insights from genetics and animal models. *Nat Rev Genet.* 2000;1:208–217.

Circulation
JOURNAL OF THE AMERICAN HEART ASSOCIATION

American Heart Association®
Learn and Live℠

Postinfarction Gene Therapy Against Transforming Growth Factor-ß Signal Modulates Infarct Tissue Dynamics and Attenuates Left Ventricular Remodeling and Heart Failure

Hideshi Okada, Genzou Takemura, Ken-ichiro Kosai, Yiwen Li, Tomoyuki Takahashi, Masayasu Esaki, Kentaro Yuge, Shusaku Miyata, Rumi Maruyama, Atsushi Mikami, Shinya Minatoguchi, Takako Fujiwara and Hisayoshi Fujiwara

Circulation 2005;111;2430-2437; originally published online May 2, 2005;
DOI: 10.1161/01.CIR.0000165066.71481.8E
Circulation is published by the American Heart Association. 7272 Greenville Avenue, Dallas, TX 72514
 Print ISSN: 0009-7322. Online ISSN: 1524-4539

Postinfarction Gene Therapy Against Transforming Growth Factor-β Signal Modulates Infarct Tissue Dynamics and Attenuates Left Ventricular Remodeling and Heart Failure

Hideshi Okada, MD; Genzou Takemura, MD, PhD; Ken-ichiro Kosai, MD, PhD; Yiwen Li, MD, PhD; Tomoyuki Takahashi, PhD; Masayasu Esaki, MD; Kentaro Yuge, MD, PhD; Shusaku Miyata, MD; Rumi Maruyama, BS; Atsushi Mikami, MD, PhD; Shinya Minatoguchi, MD, PhD; Takako Fujiwara, MD, PhD; Hisayoshi Fujiwara, MD, PhD

Background—Fibrosis and progressive failure are prominent pathophysiological features of hearts after myocardial infarction (MI). We examined the effects of inhibiting transforming growth factor-β (TGF-β) signaling on post-MI cardiac fibrosis and ventricular remodeling and function.

Methods and Results—MI was induced in mice by left coronary artery ligation. An adenovirus harboring soluble TGF-β type II receptor (Ad.CAG-sTβRII), a competitive inhibitor of TGF-β, was then injected into the hindlimb muscles on day 3 after MI (control, Ad.CAG-LacZ). Post-MI survival was significantly improved among sTβRII-treated mice (96% versus control at 71%), which also showed a significant attenuation of ventricular dilatation and improved function 4 weeks after MI. At the same time, histological analysis showed reduced fibrous tissue formation. Although MI size did not differ in the 2 groups, MI thickness was greater and circumference was smaller in the sTβRII-treated group; within the infarcted area, α-smooth muscle actin–positive cells were abundant, which might have contributed to infarct contraction. Apoptosis among myofibroblasts in granulation tissue during the subacute stage (10 days after MI) was less frequent in the sTβRII-treated group, and sTβRII directly inhibited Fas-induced apoptosis in cultured myofibroblasts. Finally, treatment of MI-bearing mice with sTβRII was ineffective if started during the chronic stage (4 weeks after MI).

Conclusions—Postinfarction gene therapy aimed at suppressing TGF-β signaling mitigates cardiac remodeling by affecting cardiac fibrosis and infarct tissue dynamics (apoptosis inhibition and infarct contraction). This suggests that such therapy may represent a new approach to the treatment of post-MI heart failure, applicable during the subacute stage. **(*Circulation*. 2005;111:2430-2437.)**

Key Words: heart failure ■ gene therapy ■ myocardial infarction ■ transforming growth factors

Myocardial infarction (MI) often leads to left ventricular (LV) remodeling, which is characterized by ventricular dilatation, diminished cardiac performance, and poor recovery of function.[1] Thus, patients who escape death during the acute stage of a large MI are at high risk of developing heart failure during the chronic stage. Indeed, patients with postinfarction heart failure account for nearly half of the candidates for cardiac transplantation.[2] The extent of the cardiomyocyte death during the acute stage of MI is a critical determinant of the subsequent ventricular remodeling and eventual heart failure, but the complex process of cardiac remodeling is not determined solely by that; hypertrophic responses occur in cardiomyocytes in the surviving portion of the ventricle, followed by ventricular dilatation due to architectural rearrangement of the cardiomyocytes and interstitial cells making up the myocardium.[3–5] In that regard, myocardial fibrosis is one of the most characteristic structural changes in infarcted hearts and contributes to both systolic and diastolic dysfunction.[6,7]

See p 2416

Several lines of evidence point to the critical role played by transforming growth factor-β (TGF-β) during the progression of myocardial fibrosis: (1) TGF-β1 induces increases in both the production and secretion of collagen, increases the abundance of collagen type I and III mRNA in cultured rat cardiac fibroblasts, and stimulates the expression of extracellular matrix proteins in vivo[8]; (2) in vivo gene transfer of TGF-β1 can induce myocardial fibrosis[8]; (3) expression of TGF-β is markedly increased in both infarcted and noninfarcted areas

Received August 11, 2004; revision received January 4, 2005; accepted January 6, 2005.

From the Second Department of Internal Medicine (H.O., G.T., Y.L., M.E., S. Miyata, R.M., S. Minatoguchi, H.F.) and Department of Gene Therapy and Regenerative Medicine (K.K., T.T., K.Y., A.M.), Gifu University School of Medicine, Gifu; and Department of Food Science, Kyoto Women's University, Kyoto (T.F.), Japan.

Correspondence to Hisayoshi Fujiwara, MD, PhD, Second Department of Internal Medicine, Gifu University School of Medicine, 1-1 Yanagido, Gifu 501-1194, Japan. E-mail gifuim-gif@umin.ac.jp

Circulation is available at http://www.circulationaha.org

DOI: 10.1161/01.CIR.0000165066.71481.8E

of hearts after MI[9,10]; and (4) TGF-β is associated with angiotensin II–mediated fibrosis, whereas inhibition of angiotensin II signaling mitigates post-MI cardiac remodeling and improves function.[11,12] Collectively, these findings suggest strongly that TGF-β plays a critical role during the healing process after MI and thus affects cardiac remodeling and function during the chronic stage.

Soluble TGF-β type II receptor (sTβRII) inhibits the action of TGF-β, most likely by adsorbing TGF-β or by acting as a dominant negative receptor.[13] In the present study we hypothesized that postinfarction treatment with sTβRII would mitigate chronic heart failure by affecting the LV remodeling process. We therefore constructed a recombinant adenoviral vector expressing the extracellular domain of the TGF-β type II receptor fused to human immunoglobulin Fc and started its transduction into mouse hindlimbs (systemic transfection) on the third day after MI, a time when therapy would not affect acute ischemic death of cardiomyocytes. We then examined the effects on LV structure and function during the chronic stage of MI and sought possible mechanisms responsible for our observations made both in vitro and in vivo.

Methods

Replication-Defective Recombinant Adenoviral Vectors

A replication-defective adenoviral vector, Ad-TβRIIEx-Fc, which expresses the extracellular domain of the type II TGF-β receptor[13] fused to the Fc portion of human IgG1 under the transcriptional control of cytomegalovirus immediate early enhancer and a modified chicken β-actin promoter, was constructed by in vitro ligation as previously described.[14] Likewise, control Ad-LacZ was prepared as previously described.[15,16]

Measurement of sTβIIR in Plasma

Plasma concentrations of sTβRII after adenoviral transfection were measured in mice (n=5) by detecting human IgG-Fc with the use of an enzyme-linked immunosorbent assay (Institute of Immunology).

Experimental Protocols

The study was approved by our institutional animal research committee. MI was induced in 10-week-old male C57BL/6J mice (Chubu Kagaku, Nagoya, Japan) by ligating the left coronary artery as previously described.[14] In sham-operated mice, the suture was passed but not tied. Ad.CAG-sTβRII (1×10^{11} particles per mouse) was then injected into the hindlimb muscles of the mice. As a control, adenovirus harboring the LacZ gene (Ad.CMV-LacZ) was injected in the same manner.

Protocol 1 (Treatment at Subacute Stage)

MI was induced in 75 mice. Of those, 55 survived to the third day after MI and were entered into the study. They were then randomly assigned into sTβRII (n=27) and LacZ (n=28) treatment groups and were followed up for 4 weeks after MI. Fifteen sham-operated mice were subjected to either of the treatments (LacZ, n=7; sTβRII, n=8) and similarly assessed. In another experiment, on the third day after MI, 10 mice were divided into sTβRII and LacZ treatment groups (n=5 each), and the survivors (n=4 in the sTβRII group and n=3 in the LacZ group) were euthanized on day 10 after MI.

Protocol 2 (In Vitro Experiment)

MI was induced in mice, and 10 days later cardiac myofibroblasts were obtained from the infarcted areas of the hearts according to the method previously described with modification.[16] Briefly, the heart was resected, and the infarcted area was removed. The tissue was then minced and incubated with collagenase type II (Worthington) in Krebs-Ringer buffer for 30 minutes at 37°C. The dissociated cells were plated on 10-cm dishes for 1 hour and then rigorously washed with buffer. The attached remaining nonmyocytes were cultured in DMEM supplemented with 5% mouse serum, which was obtained from mice 7 days after transfection with Ad.CAG-TβRII or Ad.CMG-LacZ. The cells were used for experimentation during the second and third passages. More than 90% of the cells were found to be α-smooth muscle actin (SMA) positive. A mixture of agonistic anti-Fas antibody (1 μg/mL; Pharmingen) and actinomycin D (0.05 μg/mL; Sigma) was applied for 24 hours to induce apoptosis.[17]

Protocol 3 (Treatment at Chronic Stage)

MI was induced in 33 mice that were subsequently observed for 4 weeks with no treatment. At that time, scarring was well established in the infarcts of the 25 surviving mice, and gene treatment with LacZ (n=11) or sTβRII (n=14) was started. These mice were then examined after an additional 4 weeks (8 weeks after MI). In another set of animals, we evaluated sTβRII in the 5-week-old infarcted area (1 week after viral injection) by Western blot using LacZ gene– and sTβRII gene–treated hearts (n=3 each). This was to confirm accessibility of sTβRII into scar tissue.

Physiological Studies

Echocardiograms were recorded 4 weeks after MI with the use of an echocardiographic system (Aloka) equipped with a 7.5-MHz imaging transducer. The right carotid artery was then cannulated with a micromanometer-tipped catheter (SPR 407, Millar Instruments) that advanced into the left ventricle via the aorta for recording pressures and ±dP/dt.

Histological Analysis

After the physiological analyses, all surviving mice were euthanized, and their hearts were removed. The excised hearts were cut into 2 transverse slices; the basal specimens were fixed in 10% buffered formalin and embedded in paraffin, after which 4-μm-thick sections were stained with hematoxylin-eosin, Masson's trichrome, and Sirius red F3BA (0.1% solution in saturated aqueous picric acid) (Aldrich).[14] Quantitative assessments of cell size, cell population, and fibrotic area were performed on 20 randomly chosen high-power fields (HPF) in each section with the use of a LUZEX F multipurpose color image processor (Nireco). Quantitative assessments of cardiomyocyte size (as the transverse diameter), cell population, vessel population, and fibrotic area were performed on 20 randomly chosen HPF in each section with a LUZEX F multipurpose color image processor (Nireco). The number of cardiomyocytes evaluated was 198±12 cells per heart. Vessels were identified as the lumens outlined by Flk-1–positive endothelial cells on the Flk-1–immunostained sections.

Immunohistochemical Analysis

Deparaffinized 4-μm-thick sections or cultured cells were incubated with primary antibody against α-SMA (Sigma), Flk-1 (Santa Cruz), or pan-leukocyte antigen (CD45, Pharmingen), after which they were immunostained with diaminobenzidine hydrochloride or labeled with immunofluorescent Alexa Fluor 488 or 568 (Molecular Probes). Nuclei were stained with hematoxylin or Hoechst 33342.

Apoptosis was evaluated with the use of the in situ terminal deoxynucleotidyl transferase–mediated nick-end labeling (TUNEL) method with an ApopTag kit (Intergene) as previously described.[14]

For double immunofluorescence, tissue sections or cells were stained first with the use of an FITC-conjugated ApopTag kit (Integene) and then with anti–α-SMA or anti–Flk-1 followed by labeling with Alexa Fluor 568.

Western Blotting

Proteins (100 μg) extracted from hearts in protocol 1 were subjected to 14% polyacrylamide gel electrophoresis and then transferred onto polyvinylidene difluoride membranes. The membranes were then probed with the primary antibody against matrix metalloproteinase-2 (MMP-2) (Daiichi Fine Chemical Co) or atrial natriuretic peptide (ANP) (Santa Cruz).

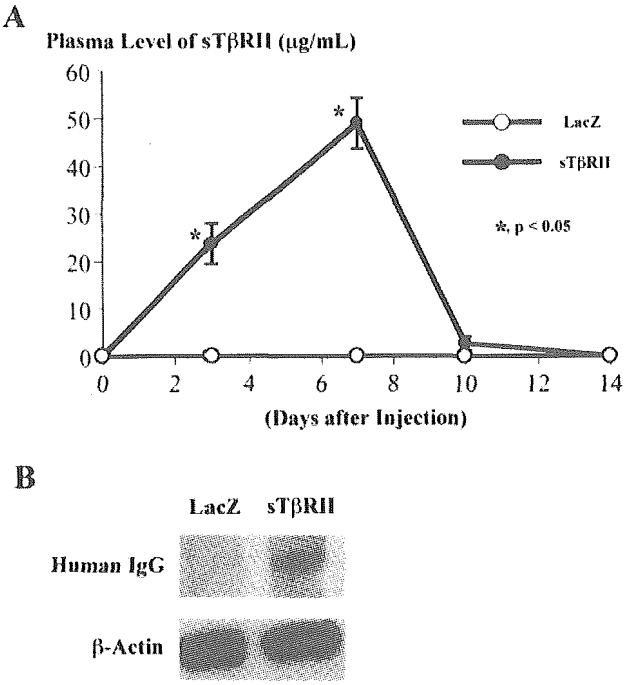

Figure 1. A, Time courses of changes in sTβRII levels measured by enzyme-linked immunosorbent assay in plasma from mice transfected with the LacZ or sTβRII gene. B, Expression of sTβRII protein in infarcted tissues as detected by anti-human IgG.

Infarct tissues were subjected to Western blotting for sTβRII by anti-human IgG antibody (DAKO).

The blots were visualized by means of chemiluminescence (ELC, Amersham), and the signals were quantified by densitometry. β-Actin (analyzed with antibody from Sigma) was the loading control.

Statistical Analysis

Values are shown as mean±SEM. Survival was analyzed by the Kaplan-Meier method with the log-rank Cox-Mantel method. The significance of differences was evaluated with Student *t* tests. Values of $P<0.05$ were considered significant.

Results

Plasma Levels of Exogenous sTβRII

Among mice receiving sTβRII gene transfection, the plasma levels of exogenous sTβRII reached 23.7±4.3 and 49.0±5.4 μg/mL, respectively, 3 and 7 days after the injection (6 and 10 days after MI, respectively), a time when the infarcted area was composed of granulation tissue (Figure 1A). Levels declined steeply thereafter, and sTβRII was undetectable in the plasma 2 weeks after MI. No sTβRII was detected in the LacZ-treated mice at any time. Accessibility of sTβRII into scar tissue was confirmed by Western blotting (Figure 1B). All sham-operated mice survived until 4 weeks after surgery.

Effect of Anti–TGF-β Treatment at Subacute Stage (Protocol 1)

Four Weeks After MI

The survival rate was significantly higher among sTβRII-treated mice than among LacZ-treated control mice 4 weeks after MI (Figure 2A): 26 of 27 mice (96%) in the sTβRII-

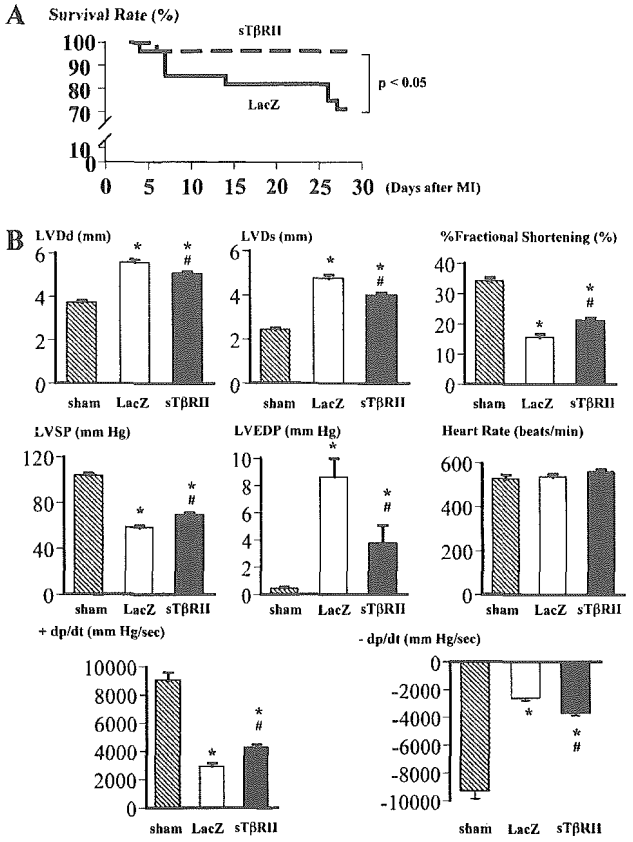

Figure 2. Survival, LV geometry, and LV function during the chronic stage (4 weeks after MI) in MI-bearing mice receiving gene therapy on day 3 after MI. A, Post-MI survival curves for LacZ-treated and sTβRII-treated mice. B to G, Effects of sTβRII therapy on cardiac anatomy and function 4 weeks after MI. LVDd and LVDs indicate left ventricular end-diastolic and end-systolic diameter, respectively; LVSP and LVEDP, left ventricular peak systolic and end-diastolic pressure, respectively; sham, sham-operated control group with LacZ gene treatment. *$P<0.05$, significant difference compared with sham; #$P<0.05$, significant difference compared with the LacZ-treated MI group.

treated group survived versus 20 of 28 mice (71%) in the control group ($P<0.05$).

Echocardiography and cardiac catheterization performed 4 weeks after MI showed control mice to have severe LV remodeling with marked enlargement of the LV cavity and signs of reduced cardiac function compared with the sham-operated mice (Figure 2B): decreased LV percent fractional shortening and ±dP/dt and increased LV end-diastolic pressure. These parameters were all attenuated in sTβRII-treated mice (Figure 2B), indicating mitigation of postinfarct remodeling and improved cardiac function. In the sham-operated mice, there was no significant difference in cardiac function 4 weeks after surgery between the sTβRII gene– and LacZ gene–treated group, indicating a negligible effect of sTβRII treatment on cardiac function of sham-operated mice (data not shown).

There was no significant difference in heart weights (Lac Z, 166±9 mg versus sTβRII, 168±6 mg) or in ratios of heart weight to body weight (Lac Z, 6±0.2 mg/g versus sTβRII, 6±0.3 mg/g) between the groups. Although hearts from LacZ-treated mice showed marked LV dilatation with a thin

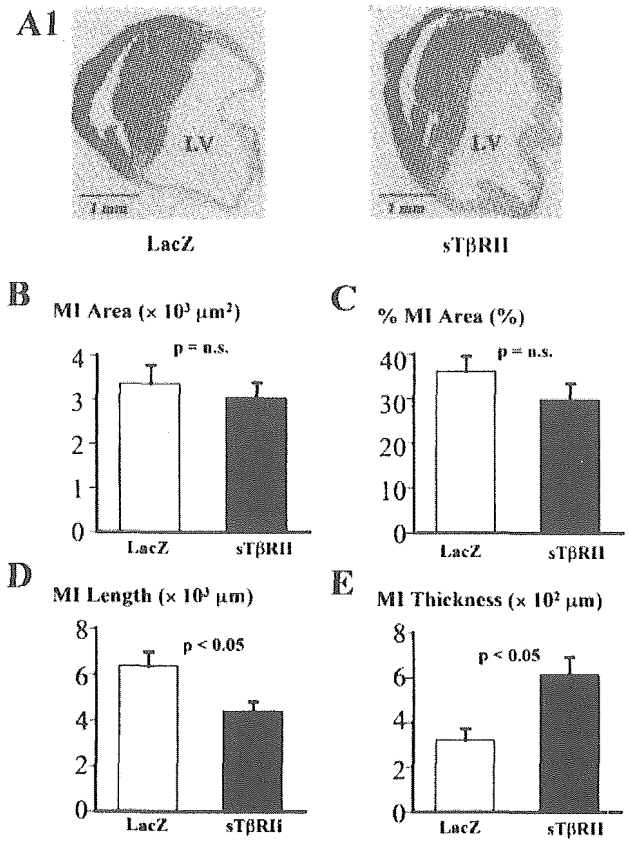

Figure 3. Morphometry of mouse hearts 4 weeks after MI. A, Transverse sections of hearts from mice treated with LacZ (A1) or sTβRII (A2). The sections are stained with Masson's trichrome. Note the smaller LV cavity, shorter infarct segment, and thicker infarct wall in the post-MI heart treated with sTβRII compared with the control heart. B, Absolute area of infarct. C, Percent area of left ventricle taken up by infarct. D, Thickness of infarct. E, Circumferential length of infarct segment.

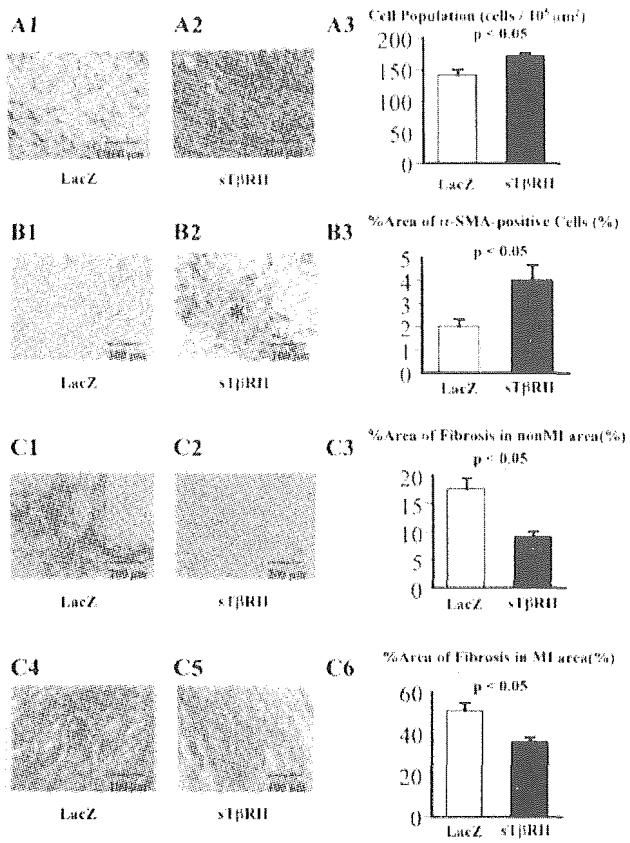

Figure 4. Histological and immunohistochemical preparations from mouse hearts collected 4 weeks after MI. A, Infarcted areas in hearts from LacZ-treated (A1) and sTβRII-treated (A2) mice; graph shows cell density (A3). Sections are stained with hematoxylin-eosin. B, Immunohistochemical analysis of α-SMA within infarcted areas of LacZ-treated (B1) and sTβRII-treated (B2) mice; graph shows percentage of infarcted area taken up by α-SMA–positive cells (B3). Asterisk in B2 indicates a bundle of α-SMA–positive cells. C, Sirius red–stained preparations of noninfarcted (C1 and C2) and infarcted (C4 and C5) areas in LacZ-treated (C1 and C4) and sTβRII-treated (C2 and C5) mice; graphs show percentage of noninfarcted (C3) and infarcted (C6) areas taken up by collagen fibers.

infarcted segment 4 weeks after MI, those from sTβRII-treated mice presented smaller LV cavities (Figure 3A1 and 3A2). Both the absolute area of the infarct and the percentage of the whole LV area taken up by the infarct were comparable between the LacZ- and sTβRII-treated mice (Figure 3B and 3C). On the other hand, the circumferential length of the infarcted segment was shorter and the infarct was thicker in the sTβRII-treated mice (Figure 3D and 3E).

By 4 weeks after MI, the infarcted areas of LacZ-treated mice had been replaced by fibrous scar tissue (Figure 4A1). The infarcts of sTβRII-treated mice, by contrast, contained not only collagen fibers but also numerous cells (Figure 4A2). The noncardiomyocyte population in the infarcted areas was significantly greater in the sTβRII-treated mice (Figure 4A3), as was the percent infarcted area taken up by extravascular α-SMA–positive cells (Figure 4B1 to 4B3). Some α-SMA–positive cells accumulated and formed bundles to run parallel with the infarct wall circumference (Figure 4B2) that were not observed in the infarcted LV walls of the control mice. Still, the population of vessels was comparable in the 2 groups (LacZ, 7.2±0.7 vessels per HPF versus sTβRII, 6.9±0.8 vessels per HPF; P=NS). There was no significant difference in population of CD45-positive cells between the control (0.9±0.1 cells per HPF) and sTβRII-treated hearts (0.8±0.2 cells per HPF; P=NS). The amount of fibrosis assessed in Sirius red–stained sections was significantly reduced in the noninfarcted LV walls and in the infarct region of the sTβRII-treated mice (Figure 4C1 to 4C6). MMP-2 in hearts with 4-week-old MI was greater in hearts with MI compared with the sham-operated hearts, but it was not significantly affected by the sTβRII treatment (Figure 5A and 5B), suggesting a negligible association of the gelatinase activity with sTβRII-induced antifibrosis in the present experimental setting. In addition, the transverse diameters of cardiomyocytes in the noninfarcted areas were significantly greater in the LacZ-treated (17.7±0.3 μm) than in the sTβRII-treated (15.1±0.3 μm) mice (Figure 5C), suggesting that the compensatory cardiomyocyte hypertrophy was more developed in the control mice. Consistent with this finding, Western blot analysis revealed reduced ANP expression in the sTβRII-treated hearts (Figure 5A and 5B).